CHARACTERIZING WINTERTIME AEROSOL COMPOSITION AND SULFATE FORMATION IN FAIRBANKS, ALASKA

By

Ragen M. Davey, B.S.

A Thesis Submitted in Partial Fulfillment of the Requirements

for the Degree of

Master of Science

in

Chemistry: Environmental

University of Alaska Fairbanks

May 2020

APPROVED:
Dr. Jingqiu Mao, Committee Chair
Dr. William R. Simpson, Committee Member
Dr. Jennifer J. Guerard, Committee Member
Dr. Thomas K. Green, Chair
Department of Chemistry & Biochemistry
Dr. Kinchel C. Doerner, Dean
College of Natural Science and Mathematics
Dr. Michael Castellini,
Dean of the Graduate School

Abstract

The citizens of Fairbanks, Alaska are exposed to high levels of air pollutants throughout the winter months, causing the city to violate the Fine Particulate Matter ($PM_{2.5}$) National Ambient Air Quality Standards set in place by the United States Environmental Protection Agency. Previous studies have shown the significant amount of sulfate aerosols particles observed in Fairbanks winters, but the formation mechanism of aerosols containing sulfate in the atmosphere is still unknown. While sulfate aerosol particle formation is commonly driven by oxidants including •OH, H_2O_2 and O_3, these photochemical species are limited in Fairbanks winter months. This indicates sulfate aerosol particle formation may occur through a non-traditional pathway, and this project investigates one proposed mechanism in which transition metals may catalyze sulfate aerosol particle formation. We collected twelve full diurnal cycles over the winter months of 2019, using a particle-to-liquid sampler (PILS) at hourly time resolution. This PILS instrument creates an aqueous extract containing only the water-soluble components of the aerosol particles. These aqueous extracts were analyzed offline for inorganic and metal concentrations by ion chromatography (IC) and inductively coupled plasma mass spectrometry (ICP-MS). This hourly dataset provides new insights in emissions, chemical processing and their coupling with boundary layer dynamics. We find a strong correlation between hourly sulfate and $PM_{2.5}$ mass concentrations, but we do not find the strong evidence of transition metal ion (TMI) catalysis on sulfate formation. We also collected twelve sets of aerosol filters using Micro-Orifice Uniform Deposit Impactor (MOUDI) throughout the winter of 2019. These size-resolved filter samples suggest the presence of hydroxymethane sulfonate (HMS) in submicron particles when temperatures are below -30 °C (-22 °F), suggesting a new reservoir for sulfur compounds in Fairbanks winter and warranting further investigation.

Table of Contents

List of Figures

List of Tables

List of Appendices

Acknowledgements

I wish to acknowledge and thank each and every person who has helped me along the way throughout my academic career.

I would like to express my deepest gratitude to my graduate committee members, Dr. Jingqiu Mao, Dr. William R. Simpson and Dr. Jennifer J. Guerard for their endless support and encouragement throughout this research project and my academic career. Additionally, I would like to thank Dr. Rodney Weber and his laboratory group at the Georgia Institute of Technology for their collaboration and assistance in data collection and analysis.

Additionally, I would like to acknowledge the two undergraduates who assisted with this project, James Campbell and Kiersten Johnson, without whom this project would not have been possible.

Thank you to UAF, The Alaska Space Grant Program, Alaska NSF EPSCoR, URSA, and BLAST for funding this research, me and undergraduate students.

Likewise, many thanks to The Alaska Department of Environmental Conservation for partial funding and the donation of the sample trailer for two field seasons, along with constant field support and assistance.

This work would not have been possible without Advanced Instrumentation Laboratory and the UAF Chemistry department for their funding, support and training on instrumentation.

And finally, thank you to Kristin Gagne and Marcus Cogley for constant Chemistry office reassurance and assistance. Thank you to all the Environmental Chemistry graduate students, who provided constant support during all of our time spent in the Reichardt building. And my deepest thanks to my amazing family and close friends for nonstop sideline cheering and the endless love provided during my time as a graduate student.

Chapter 1 Introduction

1.1 Motivation and Background

Ambient air pollution across the world has become one of the highest risk factors in terms of health burdens across the world [*Brauer et al.*, 2012]. In fact, ambient particulate matter (PM) air pollution was classified as one of the three leading risk factors for global disease burden, right behind high blood pressure and tobacco smoking [*Lim et al.*, 2012]. Fine particulates have been estimated to account for 3.2 million premature deaths annually [*Holstius et al.*, 2014] and seven million annual deaths are due to air pollution as a whole [*Rodriguez et al.*, 2020]. As research continues to show that PM air pollution pose a serious threat to public health, the United States Environmental Protection Agency (EPA) has lowered the 24-hour National Ambient Air Quality Standard (NAAQS) limit to 35 micrograms of particulate matter with a diameter less than 2.5 μm ($PM_{2.5}$) per cubic meter of air (μg m^{-3}) in 2007 [*EPA*, 2018; 2019].

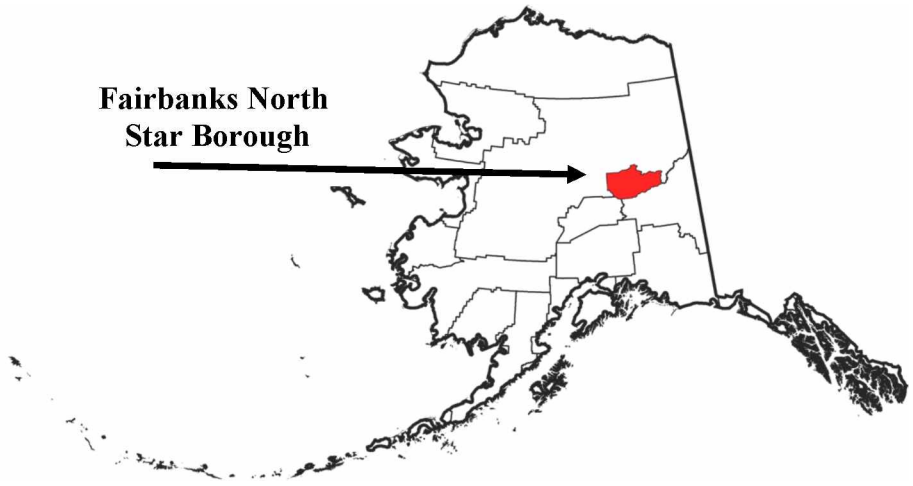

Figure 1.1: Location of the Fairbanks North Star Borough in Alaska.

Particulate matter (PM) particles are categorized under different classifications in relation to their diameter sizes [*Kleeman et al.*, 1999]. PM with a diameter less than 2.5 μm ($PM_{2.5}$) has been

identified as the highest risk to human health, in relation to particulate matter in the atmosphere [*Kleeman et al.*, 1999]. It has been shown that the adverse health effects, mainly respiratory and cardiovascular, are directly correlated to the smaller diameter particles [*Erkens and Kelm*, 2020; *Stölzel et al.*, 2007]. Because of the small size, $PM_{2.5}$ is easily inhaled and can travel into the body through the respiratory system whereas larger particles would be expelled.

Fine particulate matter causes both acute and chronic effects that harm multiple human organs [*Seaton et al.*, 1995]. Cardiac cancer, chronic bronchitis and even premature death have all been observed as results from $PM_{2.5}$ pollution [*Kampa and Castanas*, 2008; *Seaton et al.*, 1995]. Additionally, high risk individuals, such as pregnant women and the young and elderly, are all at an elevated risk to the hazardous conditions associated with particulate atmospheric pollution [*Sun et al.*, 2010]. The Women's Health Initiative Study revealed there is a 24% increase in cardiovascular events and a 76% increase in cardiovascular mortality per 10 $\mu g\ m^{-3}$ increase in $PM_{2.5}$ through the analysis of over 60,000 postmenopausal women with no previous heart conditions over six years [*Anderson et al.*, 2012; *Miller et al.*, 2007]. While there is much interest in the effects of PM on the cardiovascular system, studies also show a correlation of increased $PM_{2.5}$ exposure and respiratory illness. Minor irritation of the respiratory system in addition to chronic respiratory diseases, such as asthma, are common with hazardous air pollution [*Kampa and Castanas*, 2008]. Part of the Children's Health Study shows large increases in asthma symptoms with increased PM levels [*Slaughter et al.*, 2003] in addition to a 40% increase in bronchitis symptoms during a 19 $\mu g\ m^{-3}$ increase in PM_{10} [*McConnell et al.*, 2003]. There is also evidence of increases of respiratory medication increase in Alaska [*Chimonas and D. Gessner*, 2007] and cardiovascular medication increase among the rest of the US [*Deen et al., 2017*; *Weber et al.*, 2016].

1.2 Fairbanks $PM_{2.5}$ Pollution

With a Fairbanks North Star Borough (FNSB) population of 98,971 based on 2018 Census estimates, Fairbanks (64.83° N, 147.71° W) is the second largest city in Alaska, second to Anchorage. Fairbanks is the northernmost Metropolitan Statistical Area in the Unites States, positioned less than 190 km south of the Arctic Circle [*Wang and Hopke*, 2014]. One major issue

is that this area has been suffering from severe air pollution during winter months, posing a strong health threat to local residents [*Ward et al.*, 2012]. On average, FNSB has a large variation in daily winter $PM_{2.5}$ levels, with pollution episodes that can often exceed the NAAQS limit of 35 μg m^{-3} for a 24-hour average. The Fairbanks North Star Borough is classified as a "non-attainment" zone (Figure 1.2) for winter $PM_{2.5}$ 24-hour levels in 2009. In April of 2017, EPA officially reclassified the Fairbanks North Star Borough area from "Moderate" to "Serious" nonattainment area [*EPA*, 2018].

As shown in Figure 1.2, the FNSB area can be separated into three zones: Goldstream, Fairbanks and North Pole. We will mainly focus on Fairbanks area in this work as our measurements were mainly conducted in this area. North Pole is largely dominated by wood burning emissions Filter-based aerosol speciation measurements in downtown Fairbanks suggest that $PM_{2.5}$ aerosol mass is largely contributed by organic aerosols (50-70%) and sulfate aerosols (20%), with smaller contribution from elemental carbon and nitrate aerosols [*Nattinger*, 2016].

Figure 1.2: $PM_{2.5}$ non-attainment area in the Fairbanks North Star Borough. [*ADEC*, 2019a].

A number of source apportionment studies have been conducted in the past for Fairbanks area. Using chemical mass balance model (CMB) with EPA source profiles, Ward et al. [2012] find that wood smoke contributes to 50-70% of $PM_{2.5}$ mass in Fairbanks area, followed by sulfate (~20%), nitrate (~10%) and mobile sources (~2-8%). In a later study, Ward et al. [2012] applied source profiles measured by OMNI Environmental Services for a variety of Fairbanks-specific

home heating fuel types. They find that the contribution of wood smoke is only 30-60%, less than the results using EPA source profiles, but they attribute a significant fraction (10-47%) of $PM_{2.5}$ to No. 2 fuel oil. Wang and Hopke [2014] used the Positive Matrix Factorization (PMF) method to analyze the aerosols filters collected at State Office Building (SOB) between 2005 and 2012. They identify several major $PM_{2.5}$ sources during Fairbanks winter, including wood smoke (40%), sulfate (25%), diesel (19%), gasoline (10%) and nitrate (5%). They also find that wood smoke, sulfate and diesel were major sources to $PM_{2.5}$ mass during NAAQS violation days, with little variation between weekends and weekdays [*Wang and Hopke*, 2014]. Kotchenruther [2016] applied PMF to $PM_{2.5}$ speciation data collected near the state office building and a different period (2009-2014), and he found that primary wood smoke contributes to 40% of $PM_{2.5}$ mass, and aged wood smoke contributes to another 12% of $PM_{2.5}$ mass in Fairbanks area.

There have been several studies examining the primary emission of sulfate from Fairbanks sources using sulfate oxidation ratio (SOR). The SOR is calculated as the ratio of sulfate to the sum of sulfate and potential sulfate formed from SO_2. As the combustion of #2 heating oil is most likely the main source of sulfur in Fairbanks area. Using EPA emission factor of SO_2 and Fairbanks specific sulfate emission factor for #2 heating oil, Nattinger [2016] calculated the primary SOR from the combustion of #2 heating oil to be 2-8%. Using ambient sulfate and SO_2 data, they find the ambient SOR is 5-6% in Fairbanks winter, well within the range of primary SOR (2-8%). However, the EPA measurements were not conducted at Fairbanks conditions and thus cannot be directly applied to the Fairbanks dataset.

Overall, all source apportionment studies have shown a major contribution of wood smoke to fine particles in Fairbanks winter, followed by sulfate. To what extent sulfate is primarily emitted or secondarily formed in the atmosphere is a great motivation for this study. A better understanding of sulfate sources and transformation mechanism is crucial in developing mitigation strategies for long-term attainment of $PM_{2.5}$.

1.3 Sulfur Oxidation

The combustion of sulfur containing fuel releases mostly (~95%) sulfur dioxide gas (SO_2). Subsequently, SO_2 can be oxidized from S(IV) to S(VI) in the atmosphere, leading to the

formation of sulfate aerosols. Traditional understanding of this conversion includes three pathways. The first one is, SO_2 reacts with ambient hydroxy radical (OH), leading to the formation of sulfuric acid (H_2SO_4), and H_2SO_4 then condense to aerosols and become sulfate. The other two involves heterogeneous chemistry of cloud droplets (with a diameter of ~10 μm). SO_2 is first partitioned to aqueous phase and then reacts with aqueous hydrogen peroxide (H_2O_2) or ozone (O_3) oxidation, leading to the formation of S(VI) in aqueous droplets. As droplets evaporate, the S(VI) becomes sulfate aerosols. Due to the low photon flux and limited O_3 concentrations resulting from nitric oxide (NO), we expect these traditional pathways are unlikely to be the dominant mechanism of secondary sulfate formation in Fairbanks winter [*Joyce et al.*, 2014].

One non-traditional pathway for sulfur oxidation is, sulfur oxidation by O_2 in aqueous phase catalyzed by transition metal ions (TMI). One possible mechanism involving Fe is [*Deguillaume et al.*, 2005]:

$$Fe(III) + HSO_3^- \rightarrow Fe(II) + SO_3^- + H^+$$
$$SO_3^- + O_2 \rightarrow SO_5^-$$
$$SO_5^- + Fe(II) + H^+ \rightarrow HSO_5^- + Fe(III)$$
$$HSO_5^- + Fe(II) \rightarrow SO_4^- + OH^- + Fe(III)$$
$$SO_4^- + Fe(II) \rightarrow SO_4^{2-} + Fe(III)$$

Other transition metals may also contribute to sulfur oxidation in a similar manner, such as manganese (Mn) and copper (Cu) [*Berglund and Elding, 1995; Conklin and Hoffmann, 1988a*]. While the importance of TMI catalysis has been confirmed in cloud droplets in previous studies [*Harris et al., 2003*], it remains unknown whether or not these TMI may play an important role in facilitating sulfate formation in aerosol phase.

1.4 Hypothesis

Fairbanks winter SO_4^{2-} aerosols are formed through TMI-Catalytical Oxidation

With the knowledge presented above that transition metal ions (TMI) might play a role in S(IV) formation, we[1] hypothesize that the unknown mechanism of sulfate aerosol particle formation in Fairbanks winter is through potential metal catalyzed reactions.

To provide potential evidence of secondary SO_4^{2-} aerosol particle formation, we collected aqueous samples during the Fairbanks winters of 2018 and 2019. Hourly time resolution samples were collected to provide further speciation of Fairbanks wintertime $PM_{2.5}$. These hourly samples will help to understand how the different $PM_{2.5}$ species behave over a daily diurnal cycle.

[1] "We" is defined in this thesis as the author and co-authors of the research that lead to this thesis. This includes Ragen Davey and Jingqiu Mao.

Chapter 2 Site Description

2.1 Fairbanks Meteorology

Fairbanks, Alaska (64.83° N, 147.71° W) is located in the Tanana Valley, in the interior of Alaska and is approximately 132.9 meters (435.9 feet) above sea level. From early November to late March, the period of daylight hours ranges from as little as 4 hours to about 10 hours. This limited amount of sunlight with temperatures that drop to -40°C or colder makes Fairbanks an optimal place to study wintertime aerosol formation. Sitting about 240 km north of the Alaska Range and approximately 430 km south of the Brooks Range, Fairbanks experiences large temperature and weather variations. This large winter temperature variation, from anywhere around 55°C below to 5°C above, reflects the difference between the frigid temperatures associated with northerly airflow coming from the dry Arctic to mild temperatures associated with the southerly airflow from the Gulf of Alaska paired with Chinook winds off the Alaska Range [*Wendler and Shulski*, 2009]. There is constant snow cover (on average, 12.5 inches for January and 17.6 inches for February; Fairbanks METAR data) in Fairbanks from October to April but limited heavy snowfall during winter months [*Mölders and Kramm*, 2010]. Additionally, wintertime surface wind speeds are typically less than 0.5 m s^{-1} [*Kankanala*, 2007]. This minimal wind activity which leads to the cold, dense air settling in the valley for weeks at a time, preventing the export of pollution that is produced in Fairbanks.

Fairbanks' high latitude location and limited sunlight during the winter leads to a negative radiation balance [*Tran and Mölders*, 2011]. This negative net radiation cools the surface to a temperature below that of the air, which in turn cools the atmosphere, creating a thermally induced inversion [*Bourne et al.*, 2010]. Warm air above the inversion can then create layers of air with a gradient of temperatures, which causes very stable conditions [*Bourne*, 2008]. This paired with the land-locked, valley location of Fairbanks leads to frequent winter inversions that are among the strongest inversions found anywhere, persisting longer than those at mid or low latitudes [*Bourne et al.*, 2010; *Wendler and Nicpon*, 1975]. Due to these severe inversions, the levels of particulates Fairbanks is exposed to can reach levels similar to large metropolitan areas [*Wendler and Nicpon*, 1975].

2.2 Sample site

All aqueous samples were collected inside a trailer located in downtown Fairbanks (809 Pioneer Road), next to the Alaska Department of Environmental Conservation (DEC) National Core Monitoring Network site (NCore). All filter samples were collected on the roof of this same trailer, with direct outside exposure. This sample site is located directly next to the Chena River, which flows west into downtown Fairbanks. The site is in the vicinity of the Fairbanks Borough government office building, a parking lot and multiple restaurants. Additionally, the site is located within a half mile of a coal-fired power station and a residential housing neighborhood known to use multiple types of heating sources. Despite the potential interferences due to these infrastructures, this site is believed to accurately represent Fairbanks pollution sources and typical wintertime air quality and was chosen due to the additional details obtained from the NCore site. This site is understood to experience some of the coldest temperatures throughout Fairbanks and is located at an elevation of 136.0 meters (446.2 feet) above sea-level. Due to the site location, the samples collected measure the boundary layer.

Figure 2.1: Sample site in relation to NCore site. The sample trailer (left) used to collect all samples used for this thesis, sitting next to the DEC NCore site (right).

2.3. NCore site

The EPA NCore site (64.84° N, 147.72° W) was established in 2010 as the primary air quality monitoring station for the city of Fairbanks. The NCore site (AQS ID 02-090-0034) is a neighborhood monitoring scale and is located 70 meters from any roadway. The site has 260 degrees of unobstructed air flow and is a minimum distance of 20 meters away from trees. By positioning the sample trailer directly next to the DEC NCore site, all sample measurements are able to be compared to analyses conducted by the DEC. All DEC measurements used in analyses for this project were provided to the public through the US EPA Air Quality System (AQS) and follow EPA data quality check guidelines [*ADEC*, 2019b]

2.3.1 NCore Measurements

This NCore site is part of the DEC national network of sites and follows the neighborhood scale for site pollutant monitors. The meteorological monitoring is representative at the microscale and all samplers or instrumentation follow EPA monitoring guidelines. All monitor separation distances are dictated by the traffic vehicles per minute (VPD) of 4865 Philips Field Road. Table 2.1 below summarizes species used in this analysis. NO_y, NO and the difference is collected at 3 meters in height, rather than the 10 meters recommended in order to remain below the low winter inversion layer. NO_2, NO_x, and NO are collected at 3 meters in height with no obstructions. O_3 is collected at 3 meters height and is spaced 75 meters to 12 meters from a building obstruction. SO_2 is collected hourly and every 5 minutes at 3 meters in height with no obstructions. Ambient temperature, wind speed and wind direction are collected at both 2 meters and 10 meters with no obstructions. Relative humidity and barometric pressure are both collected at 4 meters with no obstructions. Filter samples are collected every third day to analyze for $PM_{2.5}$ speciation through the Chemical Speciation Network (CSN) for atmospheric chemistry assessments.

2.3.2 NCore Instrumentation

Both standard conditions and local conditions of temperature and pressure are used for all NCore instrumentation. Both $PM_{2.5}$ and PM_{10} pollutants are measured continuously using a Met-One Beta-ray Attenuation Monitor (BAM) 1020 PM-Coarse System with a Sharp-Cut Cyclone (SCC). Additionally, $PM_{2.5}$ is measured daily using a Sequential Partisol 2025i with a Very

Sharp Cut Cyclone (VSCC, Thermo Scientific) and PM10 is measured every third day using a Partisol 2000i (Thermo Scientific). In Fairbanks, $PM_{2.5}$ speciation filters are measured every third day using a Met-One Super Speciation Air Sampler System (SASS) and URG-3000.

The remainder of pollutants are measured continuously by use of Thermo Scientific Trace Level-Enhanced (TLE) instruments. Meteorological measurements are also measured continuously by the use of Met-One instruments. Instrumentation and sample frequency are summarized in Table 2.1.

Table 2.1: Summary of NCORE Measurements used in this Analysis [*ADEC*, 2019b]

Species Measurement	Time Resolution	Height (m)	Instrument
$PM_{2.5}$ mass	1 hr	4.5 m	Met-One BAM 1020X Coarse
$PM_{2.5}$ mass	1/1 day	4.5 m	Thermo Scientific Sequential Partisol 2025i[1]
PM_{10} mass	1 hr	4.5 m	Met-One BAM 1020X Coarse
PM_{10} mass	1/3 day	4.5 m	Thermo Scientific Partisol 2000i
OC	1/3 day	4.5 m	URG-3000
CO	1 hr	3 m	Thermo Scientific 48i-TLE
SO_2	5 min	3 m	Thermo Scientific 43i-TLE
NO_y, NO & diff	1 hr	3 m	Thermo Scientific 42iY-TLE
NO_x, NO & diff	1 hr	3 m	Thermo Scientific 42i-TLE
O_3	1 hr	3 m	Teledyne API 400E
Ambient Temp	Continuous	2 & 10 m	Met-One Temp Sensor
WS & WD	Continuous	3 & 10 m	Met-One Sonic Anemometer
Barometric Pressure	Continuous	4 m	Met-One BAM 1020X Barometer
Relative Humidity	Continuous	4m	Met-One BAM 1020X Relative Humidity Sensor
$PM_{2.5}$ speciation[2]	1/3 day	4.5 m	Met-One Super SASS PM2.5 LC

[1]Serves as the Federal Reference Monitor (FRM) for Fairbanks.
[2]PM Spec. includes Ba, Br, Ca, Cu, Cl*, Fe, K*, Mn, Mg, Na, Na*, NH_4, NO_3, SO_4, Sr, & Zn.
*Indicates species analyzed both with XRF and IC.

Chapter 3 Methods

3.1 Sample collection, preparation and preservation

3.1.1 Aqueous sample collection

Aqueous ambient air samples were collected using a model 4001 Particle into Liquid Sampler System (PILS, Brechtel Manufacturing Incorporated). A steel rod connected the sample inlet (set at same height as NCore instrumentation, approximately 4.5 m) to PILS impactor inlet. The ambient aerosol sample flow (Table 3.1) mix with a 100 °C steam flow (1.5 L min^{-1} gas) of adiabatic cooling to grow aerosol particles into droplets (droplet size (Dp) > 1 µm.) [*Orsini et al.*, 2003]. The droplets produce a continuous liquid flow (Table 3.1) for collection of hourly samples using an auto-collector for 24 consecutive hours. In order to obtain adequate sample volume, orange-green peristaltic pump tubing was installed on the PILS instrument for the entire sample collection (bore: 0.38 mm, marprene). These samples are collected in 12 mL vials (polypropylene, contain snap cap with punched holes that are covered with Parafilm during sampling). Hourly samples (~300) were collected throughout 12 full diurnal cycles in January and February of 2019 (Table 3.2), under the manufacturer suggested operating procedure for the instrument (tip temp. avg.: 98.0 °C; steam heater temp. avg.: 105°C). The weather and air quality conditions for these diurnal cycles are further described in Table 3.3. A diagram of PILS instrument is shown in Figure 3.1 and Table 3.1 below summarizes PILS flow for the duration of the 2019 sample period.

Table 3.1: PILS Flow Rate Change from January to February

Month	Spl. Inlet Flow	Steam Flow	Cont. Air Flow	Liq. Spl. Flow[1]
January	11.2 L min^{-1}	1.5 L min^{-1}	672 L hr^{-1}	17.2 mL hr^{-1} (8.6 mL 30 min^{-1})
February	12.7 L min^{-1}	1.5 L min^{-1}	763 L hr^{-1}	14.0 mL hr^{-1} (7.0 mL 30 min^{-1})

[1]Samples were collected every thirty minutes and then combined to one vial to account for the hour sample, to collect maximum amount of sample value for analysis.

A 2.5 µm impactor is installed directly on PILS to prevent particles larger than 2.5 µm from entering the instrument sample air flow inlet. In order to remove both organic and inorganic interference due to gases, denuders were places inline immediately upstream of the PILS. Two annular glass denuders (URG-2000-30-242-3CSS) are coated with one of two solutions for the removal of gases. For the removal of acids (HNO_3, NHO_2, SO_2, acetate, HCl, formic and oxalic acid), a coating solution containing 2% sodium carbonate in a solution of 500 mL deionized water, 20 mL glycerol and 750 mL of methanol was used. For the removal of NH_3, 2% phosphoric acid is substituted for the sodium carbonate. For removal of organic gases, a cross-section aluminum organic vapor denuder containing 15 carbon-impregnated paper strips is installed upstream of the inorganic denuders.

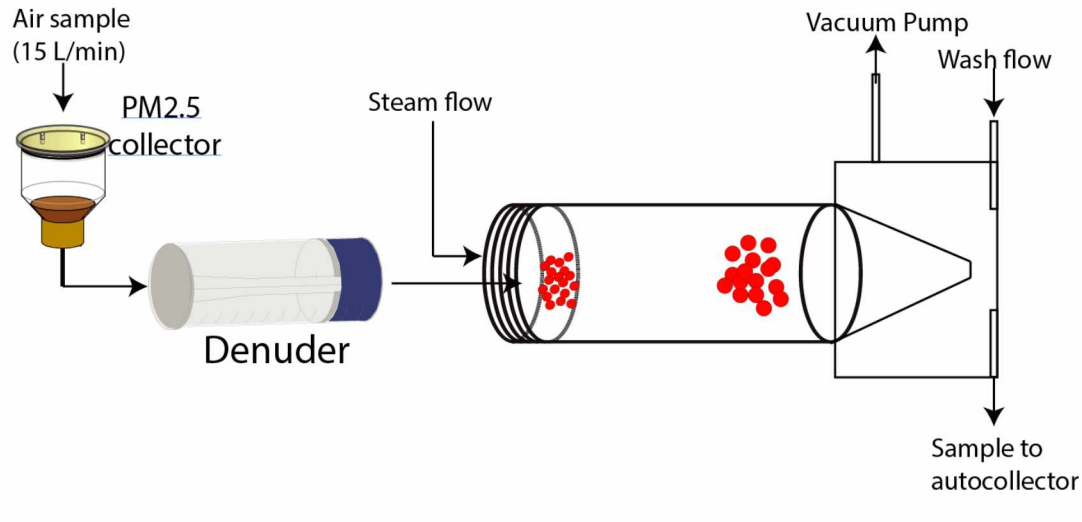

Figure 3.1 Diagram of PILS sample air flow. The denuders were arranged in the order of sample inlet – acid denuder – base denuder – organic denuder – PILS head.

Table 3.2: PILS Sample Diurnal Cycle Dates and Times

Diurnal Cycle Dates	Start Time AKST (date)	End Time AKST (date)[1]
Jan 9-10, 2019	15:40 (1/9)	18:50 (1/10)
Jan 11-12, 2019	7:55 (1/11)	8:03 (1/12)
Jan 12-13, 2019	8:03 (1/12)	8:12 (1/13)
Jan 15-16, 2019	15:37 (1/15)	22:00 (1/16)
Jan 28-29, 2019	16:13 (1/28)	17:07 (1/29)
Jan 29-30, 2019	17:07 (1/29)	17:17 (1/30)
Feb 5-6, 2019	13:37 (2/5)	13:45 (2/6)
Feb 14-15, 2019	14:40 (2/14)	14:50 (2/15)
Feb 15-16, 2019	14:50 (2/15)	14:37 (2/16)
Feb 16-17, 2019	14:39 (2/16)	14:49 (2/17)
Feb 21-22, 2019	14:55 (2/21)	15:03 (2/22)
Feb 24-25, 2019	12:52 (2/24)	15:07 (2/25)

[1]End time (AKST) delayed due to transition time to each vial, which is on average 20 seconds per vial transition. This creates the start to end time of each diurnal cycle to be delayed by ~10 minutes.

Table 3.3: Aqueous Sample Air Quality and Weather Conditions

Diurnal Cycle Date	AQI[1]	Average PM2.5 Conc. ($\mu g\ m^{-3}$)	Average Temp. (°C)	Average Wind Speed ($m\ s^{-1}$)	Observed Weather[2]
Jan 9-10	Good	6.67	-25.41	1.13	Light Snow/ Mist
Jan 11-12	Moderate	18.0	-34.50	1.10	Light Snow/ Mist
Jan 12-13	Moderate	16.89	-29.53	0.95	Mist/ Clear
Jan 15-16	Moderate/ Unhealthy sens. groups	25.04	-21.02	0.89	Clear
Jan 28-29	Moderate	12.20	-4.49	0.63	Light Snow/ Mist
Jan 29-30	Good/Moderate	11.74	-10.08	1.10	Light Snow
Feb 5-6	Good/Moderate	11.12	-8.95	0.67	Light Snow/ Cloudy
Feb 14-15	Good/Moderate	12.16	-20.72	0.92	Snow/ Shallow Fog
Feb 15-16	Good	9.47	-20.48	1.1	Light Snow
Feb 16-17	Good	9.36	-11.87	0.82	Light Snow
Feb 21-22	Moderate	10.81	-19.58	0.91	Light Snow/ Mist
Feb 24-25	Moderate	14.71	-11.52	0.65	Cloudy

[1] The average air quality index classification for $PM_{2.5}$ for the 24-hour cycle *[ADEC, 2019a].*
[2] Observed weather by author, Ragen Davey, at time of sample collection.

3.1.2 Aqueous sample preservation

Aqueous PILS samples were collected every 30 minutes for 24 consecutive hours in 18.2 MΩ washed 12 mL polypropylene vials. Upon sample completion of the 24-hour diurnal cycle, each 30-minute sample was combined to create one sample vial for every hour collected. These samples were stored in MQ washed 30 mL Nalgene^{TM} bottles (high-density polyethylene) and frozen (-18 °C) until analysis by inductively coupled plasma–mass spectrometry (ICP-MS) or ion chromatography (IC). Frozen samples were wrapped in lab-grade aluminum foil to avoid any interreference from the freezer light.

3.1.3 Blank samples and Internal Standard

Lithium bromide (LiBr, 100 ppb) was added to the wash flow in order to use the known LiBr concentration as an internal standard (ISTD). The units of ppb in this solution refers to the micrograms of solute per liter of solution. In January, the concentration of the ISTD was calculated to be 8.15 ppb Li^+ and 93.8 ppb Br^-. In February, the concentration of the ISTD was calculated to be 8.08 ppb Li^+ and 93.0 ppb Br^-. This variation in concentration is due to a new, fresh ISTD solution used for each month. When using this ISTD for correction factors (equations described in Section 3.5), the ICP-MS correction factor was used for ICP-MS cations. Similarly, the IC – Br^- correction factor was used for IC anions and the IC – Li^+ correction factor was used for IC cations.

During sample collection, an aliquot of the LiBr internal standard and MQ water was taken and stored following the same sample preservation protocol. These blank samples were analyzed using IC and ICP-MS in order to subtract out any interference added to the samples. All January blanks were averaged for blank subtraction of January samples. February blanks followed this same method. Additionally, a high-efficiency particulate air (HEPA) filter was placed on the PILS sample inlet for one hour before sample collection. This allowed for an instrument background blank sample to be collected to account for any interferences from the denuders or PILS instrument.

3.2 Filter sample collection

An MSP Corporation (Minneapolis, MN) 10 stage Micro-Orifice Uniform Deposit Impactor (MOUDI) was used to collect size-resolved aerosols for analysis. Theoretical MOUDI 50% aerodynamic diameter cut sizes of the stages are 10.00, 6.20, 3.10, 1.80, 1.00, 0.62, 0.31, 0.18, 0.10, and 0.056 µm. All samples were collected onto impaction plates containing Whatman 47 mm quartz filters at a flow rate of 30 L min^{-1} for approximately 120 hours (5 days). A $PM_{2.5}$ bulk sampler was run in unison with the MOUDI sampler to validate total PM mass was collected. These $PM_{2.5}$ mass samples were collected on Whatman 47 mm polytetrafluoroethylene (PTFE) filters (Whatman 7590-004) at an average flow rate of 17 L min^{-1} for the same sample start and end times as the MOUDI sampler. Blank filters were placed on both the MOUDI and $PM_{2.5}$ bulk sampler in order to account for any instrument background interference.

Table 3.4: Collected Filter Samples Dates

MOUDI Samples	**MOUDI and PM2.5 Bulk Samples**
Nov 15-21, 2018	Jan 30-Feb 4, 2019
Nov 26-Dec 3, 2018	*Feb 15-20, 2019
Dec 3-8, 2018	*Feb 21-26, 2019
Jan 8-13, 2019	*March 1-6, 2019
Jan 15-20, 2019	*March 7-12, 2019
Jan 24-29, 2019	*March 15-21, 2019

*Sample periods (AKST) when both MOUDI and $PM_{2.5}$ samples were collected, analyzed by mass composition.

3.3 Chemicals and reagents

Ultrapure deionized (DI) water, with resistance greater than 18 MΩ, was obtained from a Milli-Q water system (Thermo Fisher Scientific, Waltham, MA). All acids used were trace metal grade (Omnitrace or Ultrext) and purchased from Thermo Fisher Millipore Sigma (Burlington, MA).

All inductively coupled plasma-mass spectrometry (ICP-MS) standards were purchased from Agilent Technologies (Santa Clara, CA).

All ion chromatography (IC) salts were greater than 99% purity and were purchased from Thermo Fisher Scientific (CaCl, K_2SO_4, KH_2PO_4, $NaNO_3$, NH_4Cl; Waltham, MA), Alfa Aesar (NaCl; Haverhill, MA), Sigma-Aldrich (KCl, LiCl, MgCl, NaF, Na_2HPO_4 St. Louis, MO) and Mallinckrodt Chemical Works ($NaNO_2$, NaBr; St. Louis, NJ). The PILS internal standard was purchased from Sigma-Aldrich (St. Louis, MO) and PILS denuder solutions were purchased from Thermo Fisher Scientific (Waltham, MA).

3.4 Analytical methods

3.4.1 Ion analysis of aqueous samples

Cation and anion analysis of aqueous samples was performed with the IC using RTI International PM Cation Analysis and EPA Anion Method 300.0. The ion concentrations were analyzed on a Thermo-Fisher Dionex ICS 3000 (Waltham, MA) dual-column system, including: Br^-, Ca^+, Cl^-, F^-, K^+, Li^+, Mg^+, Na^+, NH_4^+, NO_2^-, NO_3^-, SO_4^- and PO_4^-. The anion system contained: an EGC III KOH cartilage (Dionex), AS18 2x250 mm column, AG18 2x50 mm guard column (IonPac) and ADRS 600 4 mm suppressor in order to analyze samples with a gradient method and 50 µL injection loop. The cation system contained: an EGC 500 MSA cartilage (Dionex), CS12A 4 x 250 mm column, CG12 4x50 mm guard column (IonPac) and CDRS 600 4 mm suppressor to analyze samples in isocratic mode using a 200 µL injection loop. Calibrations were performed at the beginning of each IC run for every ion (0.5-1000 ppb) and the calibrations for specific species are shown in Appendix A (Table A.2). In addition, appropriate method blanks and Inorganic Ventures quality control standards (Christiansburg, VA) were added in line throughout analysis. Both the anion gradient method and cation isocratic method are described in Appendix A.

3.4.2 Metal analysis of aqueous samples

An aliquot of sample was diluted to 2% HNO_3 and stored in the refrigerator (4 °C) in 8 mL polypropylene vials in preparation for analysis by ICP-MS. An Agilent 7500 ce ICP-MS (Santa

Clara, CA) was used to measure metal concentrations in PILS samples, including: Ba, Ca, Cu, Fe, K, Li, Mg, Mn, Na, Sr, and Zn. External calibration was performed at the beginning of each ICP-MS run for every element (0.01-2000ppb). In addition, appropriate internal standards were added in line throughout the analysis (Ge, Y, Sc, Rh, and Ir). Calibration checks and calibration blanks were measured every ca. 10 samples. Further, appropriate method blanks, acid blanks and reference standards (SLRS-5 riverine water and NIST 1640a trace elements in natural water systems) were analyzed with each batch of samples.

3.5 Data Analysis (Math Methods)

We download the EPA data from EPA database (https://aqs.epa.gov), using a Python code created by Mr. Alex Edwards at Alaska DEC. The EPA database allows retrieval of data with prescribed parameters. We use state code '02' for Alaska, county code '090' for FNSB county and site code '0034' for NCore site. Aerosol speciation data is available since 2013 at this site. We use the following parameters for aerosol speciation data in Table 3.5, which is available every third day for a sampling period of 24 hours. In particular, $PM_{2.5}$ data (88101) and average ambient temperature (68105) data were provided every day, every third day and every sixth day. We merged the data from different sample frequencies to minimize the missing values.

Table 3.5 EPA Daily Data

Species	EPA Code	Species	EPA Code	Species	EPA Code	Species	EPA Code
Sulfate	88403	Nitrate	88306	Chloride	88203	Ammonium	88301
$PM_{2.5}$	88101	Temperature	68105	Iron	88126	Copper	88114
Manganese	88132	Barium	88107	Strontium	88168	Zinc	88167
Magnesium	88140	Calcium	88111	Potassium (XRF)	88180	Sodium (IC)	88302
Sulfur (XRF)	88169	Chlorine (XRF)	88115	Potassium (IC)	88303	Sodium (XRF)	88184

We also retrieved hourly data from EPA database for the winter of 2019, using the parameter below. Note that we here use a different $PM_{2.5}$ mass measured by BAM for hourly data, different from FRM method in Table 3.5. The hourly temperature and wind data used in this work are based on the temperature and wind data at 3m. The hourly data is then merged with our diurnal cycle data at their corresponding hours, using MATLAB scripts.

Table 3.6 EPA Hourly Data

Species	EPA Code	Species	EPA Code	Species	EPA Code	Species	EPA Code
CO	42101	SO_2	42401	NO_y	42600	NO	42601
NO_2	42602	NOx	42603	NO_z	42612	O_3	44201
Windspeed (at 10m)	61101 (POC=1)	Windspeed (at 3m)	61101 (POC=2)	Wind direction (at 10m)	61102 (POC=1)	Wind direction (at 3m)	61102 (POC =2)
Temperature (at 10m)	62101 (POC=1)	Temperature (at 3m)	62101 (POC=2)	Relative Humidity	62201	$PM_{2.5}$	88501

POC is the "Parameter Occurrence Code" used to distinguish different instruments that measure the same parameter at the same site (https://aqs.epa.gov/aqsweb/documents/AQS_Format.html).

We measured the Li^+ and Br^- from the vial collected at the beginning of each diurnal cycle. The measured concentration of the Li^+ and Br^- will serve as the standard concentration for the internal standard correction, as shown below. The sample concentration of Li^+ and Br^- were measured from each ambient sample and the ratio of standard concentration to sample concentration will provide the correction factor for each diurnal cycle.

The lithium bromide correction factor used follows Equation 1 and 2 below. The sample concentrations were then multiplied by the diurnal LiBr correction factor to account for evaporative loss or condensational dilution of water vapor during droplet collection inside the PILS.

$$\textbf{Equation 1: } [Cation]_{Corrected} = [Cation]_{Raw}\left(\frac{[Li^+]_A}{[Li^+]_B}\right)$$

$$\textbf{Equation 2: } [Anion]_{Corrected} = [Anion]_{Raw}\left(\frac{[Br^-]_A}{[Br^-]_B}\right)$$

Where A is the concentration in the standard solution and B is the concentration analyzed in the sample.

Chapter 4 Results and Discussion: Inorganic Species

4.1 Sulfate Correlation

Sulfate aerosol mass concentrations were found to be well correlated with $PM_{2.5}$ mass concentrations during Fairbanks winter. Using the 24-hr average aerosol speciation data collected at State Office Building, Nattinger [2016] shows that sulfate appears to be well correlated with $PM_{2.5}$ mass during the period of 2006-2014. They also find that sulfate accounts for 16-19% of total $PM_{2.5}$ mass, and this ratio appears to have very little variation from year to year.

We reexamine this relationship using the wintertime aerosol speciation data collected at NCORE site during 2013-2019. This dataset is collected every 3rd day, following the same protocol as State Office Building. Similar to Nattinger [2016], we find a good correlation between sulfate and PM2.5 mass, and sulfate accounts for 20-22% of total $PM_{2.5}$ mass. Below we show the least square fit equations for correlation plots between sulfate and $PM_{2.5}$ in each individual year:

2016: $[SO_4^{2-}] = 0.21\ [PM_{2.5}] - 0.65$
2017: $[SO_4^{2-}] = 0.20\ [PM_{2.5}] - 0.32$
2018: $[SO_4^{2-}] = 0.22\ [PM_{2.5}] - 0.54$

The correlation between sulfate and $PM_{2.5}$ could point to two possibilities. One is that sulfate and $PM_{2.5}$ share the same major sources, which would suggest that sulfate is primarily emitted in Fairbanks. For example, sulfate emission from wood smoke (such as organosulfate) could help to explain such correlation, although it seems unlikely as sulfate contributes to ~20% of $PM_{2.5}$ and woodstove smoke contributes to 40-70% of $PM_{2.5}$. Another possibility is that fine particles other than sulfate, provide aerosol surface area for heterogeneous chemistry to take place, converting gaseous SO_2 to aerosol sulfate. It is possible that both primary emission and secondary formation contribute significantly to sulfate mass. It is also possible that the secondary formation may be

limited by other factors (such as aerosol acidity, aerosol surface coating, etc.). These aspects remain to be elucidated.

We find that the ratio of sulfate to $PM_{2.5}$ in recent years is slightly higher than the results from Nattinger [2016]. Such difference could be due to the difference in sampling locations, or due to the relative change in residential heating fuel type in recent years.

We further examine this correlation with PILS hourly data collected in this work and hourly $PM_{2.5}$ data provided by DEC. Figure 4.1 shows the correlation plots between hourly sulfate and hourly $PM_{2.5}$ in both January and February. Similar to 24-hr average dataset, the hourly sulfate and $PM_{2.5}$ shows good correlation, although we see more variability in hourly plots. We show that in these hourly plots, sulfate accounts for 21-22% of $PM_{2.5}$ mass, in agreement with 24-hr average dataset.

Another feature in the hourly correlation plots is that in both January and February, we show that there is another cluster of data, different from the correlated cluster that is observed in EPA trends. We find from individual diurnal cycles that these points with high $PM_{2.5}$ and low sulfate points, often occur during night or morning, are accompanied by relatively high level of SO_2. As heating oil combustion is presumably the major source of SO_2 in Fairbanks area, this cluster might represent air masses from fresh plumes from heating oil combustion. It also suggests that sulfate emission from heating oil combustion could be relatively low, providing new insights into the sulfate sources and formation mechanisms. Certain diurnal cycles where the loss of $PM_{2.5}$ and SO_4^{2-} is observed are discussed in Section 4.5.1.

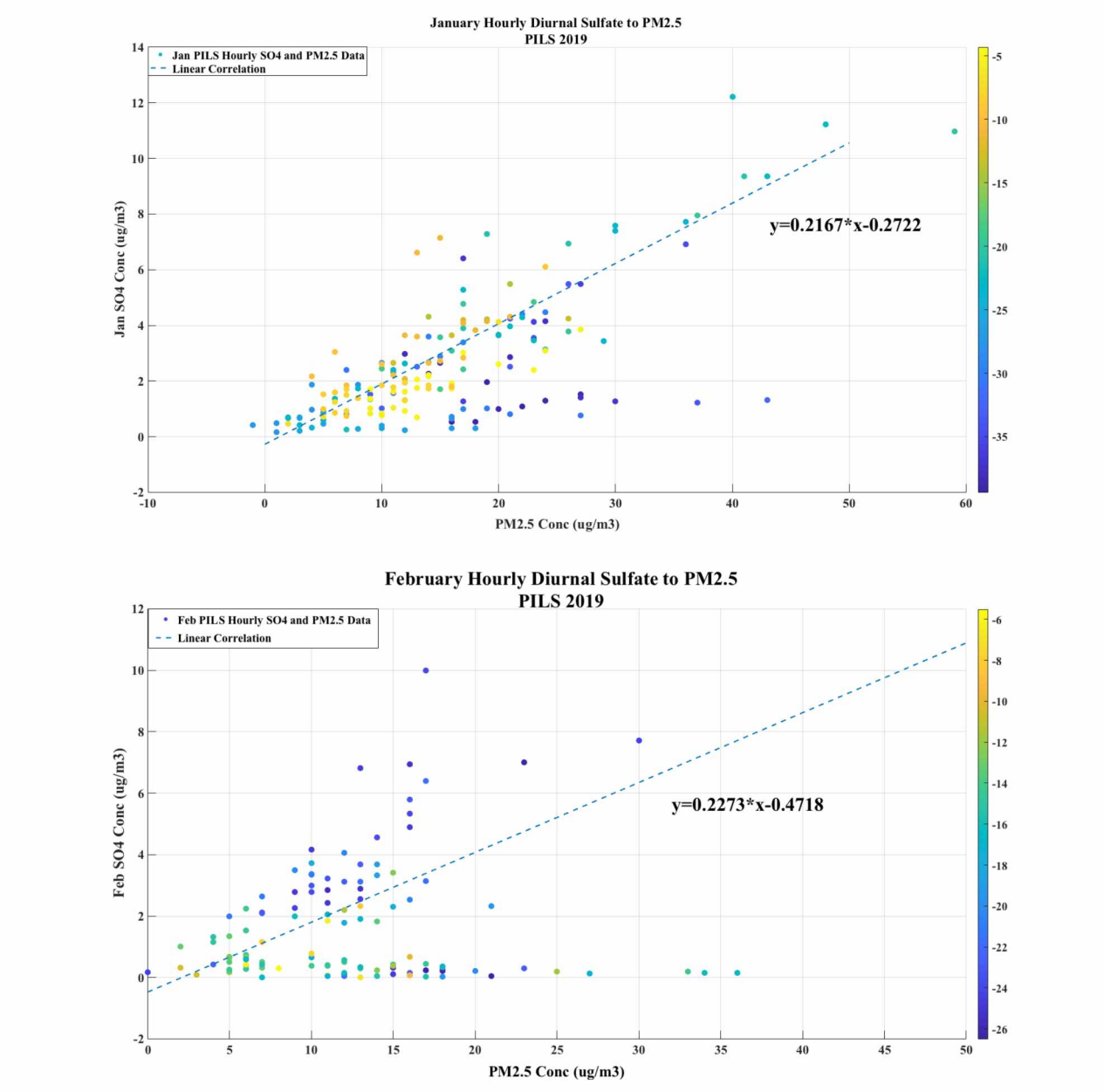

Figure 4.1: Correlation plots between hourly sulfate collected by PILS and hourly $PM_{2.5}$ mass provided by EPA, in January (upper) and February (lower) of 2019. Data points are color coded by ambient temperature (°C). The least-square fit is only applied to the upper cluster in each plot.

4.2 Statistical Species Correlation

Figure 4.2 show the January correlation matrix using a merged dataset with hourly data from DEC on $PM_{2.5}$, SO_2, O_3, NO_y and CO, and hourly PILS data, from six diurnal cycles collected in

January. This plot is produced by PRISM GraphPad software. We show that $PM_{2.5}$, SO_2, NO_y and CO all show positive correlations in January, suggesting that the variability of these species is driven by local sources and metrological variables. Additionally, ozone shows strong negative correlation with all species just mentioned, likely due to NO_x titration in shallow surface layer. All January values for Pearson R correlation coefficients are listed in Appendix B (Table B.1).

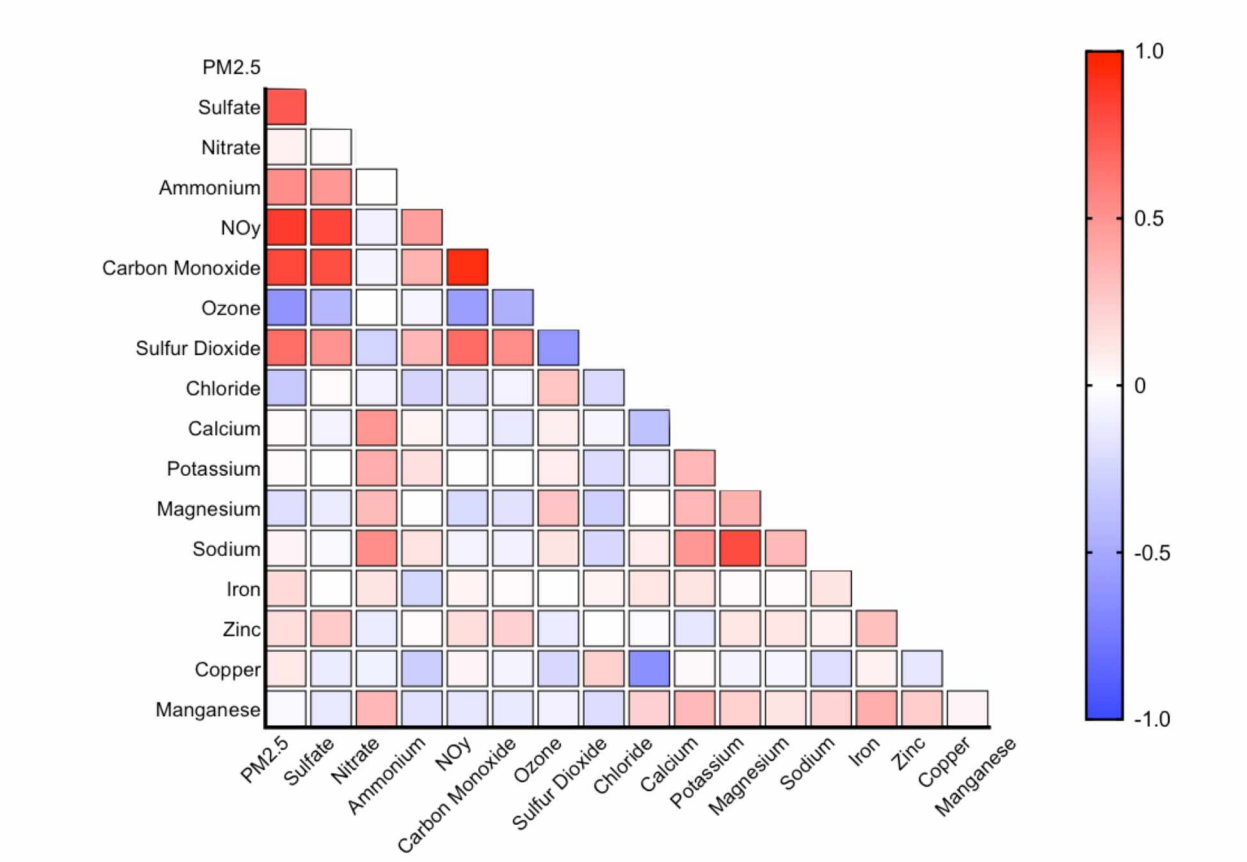

Figure 4.2: Pearson R Correlation of PILS hourly data combined with DEC measurements in January 2019. The heat map shows strong positive correlation with a dark red and strong negative correlation with a dark blue. PILS species that were measured with both IC and ICP-MS (sodium, potassium, magnesium and calcium) are represented here by their IC numbers only.

Figure 4.3 shows the February correlation matrix using the hourly merged dataset. This is similar to what is observed in January; however, ozone positively correlates with nitrate (R = 0.21). This change from January to February is consistent with stronger vertical mixing occurring into February. February values for Pearson R correlation coefficients are listed in Appendix B (Table B.2).

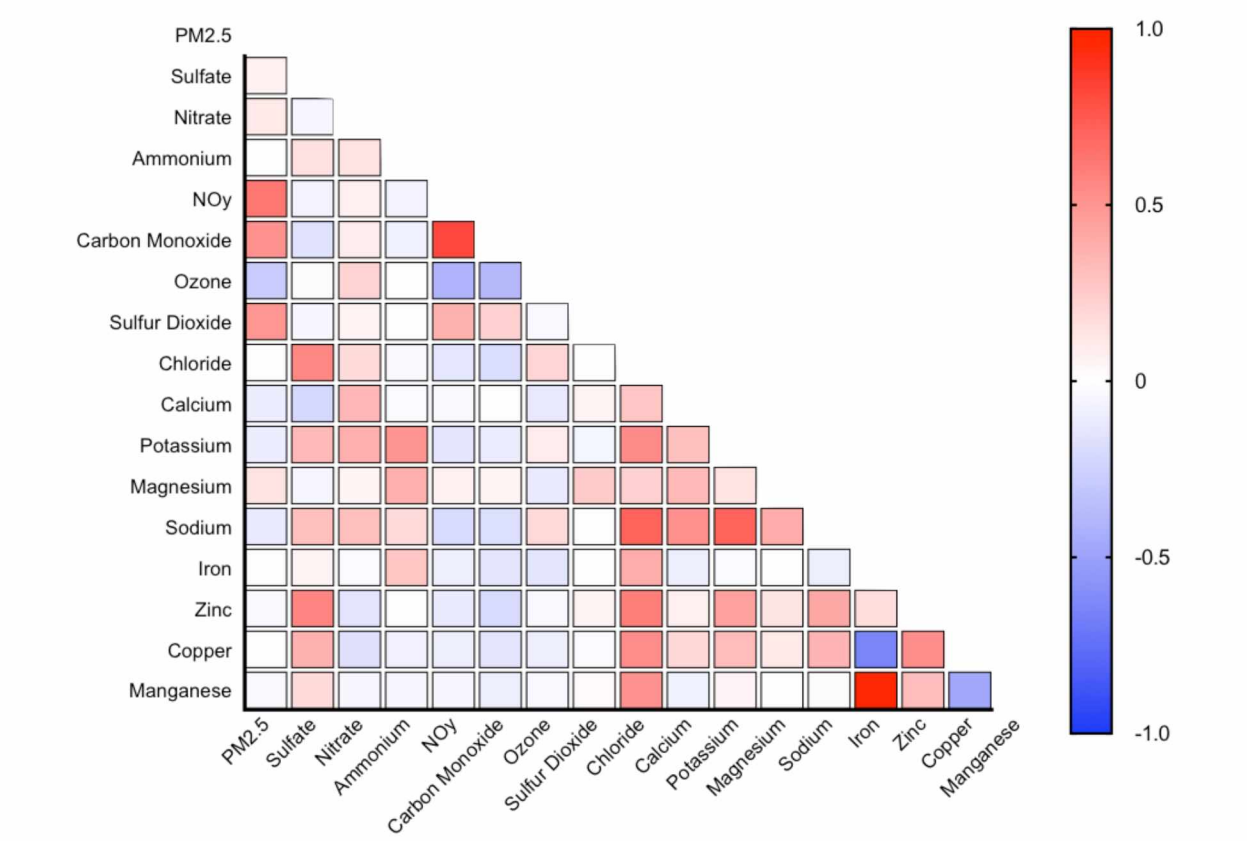

Figure 4.3: Pearson R Correlation of PILS hourly data combined with DEC measurements in February 2019. The heat map shows strong positive correlation with a dark red and strong negative correlation with a dark blue. PILS species that were measured with both IC and ICP-MS (sodium, potassium, magnesium and calcium) are represented here by their IC numbers only.

4.3 SO_2 Correlation with $PM_{2.5}$

Figure 4.4 shows a good correlation between hourly SO_2 concentrations and BAM $PM_{2.5}$ mass concentrations measured at NCORE, in both January and February. We find that the correlation between hourly SO_2 and $PM_{2.5}$ in January has a correlation coefficient R=0.67. The correlation in February is slightly better, with a correlation coefficient R=0.74. We also compute the 24-hr average for the hourly dataset and found similar correlation, consistent with Nattinger [2016].

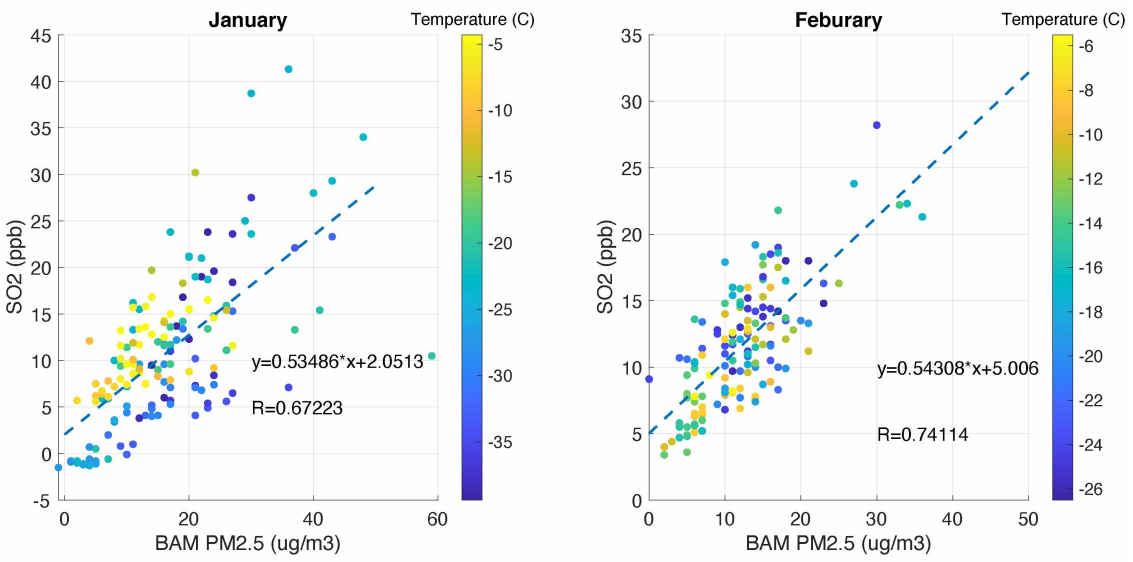

Figure 4.4 Correlation between hourly SO_2 mixing ratio and $PM_{2.5}$ mass concentrations in January (left) and February (right) of 2019. The points are colored by ambient temperature (C). The data points are selected for the time when diurnal cycle samples were collected (Table 3.2). The equations were computed for least-square fit.

In contrast to hourly data, we find a different behavior between SO_2 and $PM_{2.5}$ for diurnal cycles. As shown in Figure 4.5, the median diurnal cycle of SO_2 in January shows a nighttime peak around 2-4 am night, likely due to heating oil combustion. The median diurnal cycle of $PM_{2.5}$ shows its maximum in the evening, when woodstove emissions are likely dominating the $PM_{2.5}$ sources in Fairbanks area. This opposite diurnal patterns between SO_2 and $PM_{2.5}$ suggests poor correlation, inconsistent with the correlation plot for January in Figure 4.4. On the other hand, the median diurnal cycle of SO_2 and $PM_{2.5}$ in February show almost the same diurnal pattern, consistent with the correlation plot in Figure 4.4.

We attribute this different behavior between hourly correlation plot and median diurnal cycle of SO_2 vs. $PM_{2.5}$ in January to two reasons. First, due to lack of vertical mixing in January, diurnal variation of surface SO_2 and $PM_{2.5}$ is mainly driven by source strength and horizontal mixing. In contrast, vertical mixing is largely enhanced in February, and becomes one of the main drivers for diurnal variation for these primary pollutants, such as SO_2 and $PM_{2.5}$. Second, we notice the large difference in dynamic range between correlation plot and median diurnal cycles. We show that in hourly plots (Figure 4.4), SO_2 and $PM_{2.5}$ ranges from 0 to 40 ppb and 0 to 50 $\mu g/m^3$ respectively.

The median diurnal cycle plots show much smaller dynamic range, with 8-16 ppb for SO_2 and 11-22 $\mu g/m^3$ for $PM_{2.5}$ respectively. The hourly correlation plots shown in Figure 4.4 includes both polluted and clean episodes, resulting in a large variance between SO_2 and $PM_{2.5}$ and leading to a positive correlation. On the other hand, the dynamic range is much smaller in median diurnal cycles. On averaging basis, the main sources of SO_2 and $PM_{2.5}$ peak at different hours of the day, leading to poor correlation between these two species on diurnal cycle. In contrast, the diurnal cycle plots are consistent with hourly correlation plots in February, when SO_2 and $PM_{2.5}$ have similar dynamic range in both plots, and they are strongly driven by meteorological field such as vertical mixing and wind events that clean out the basin.

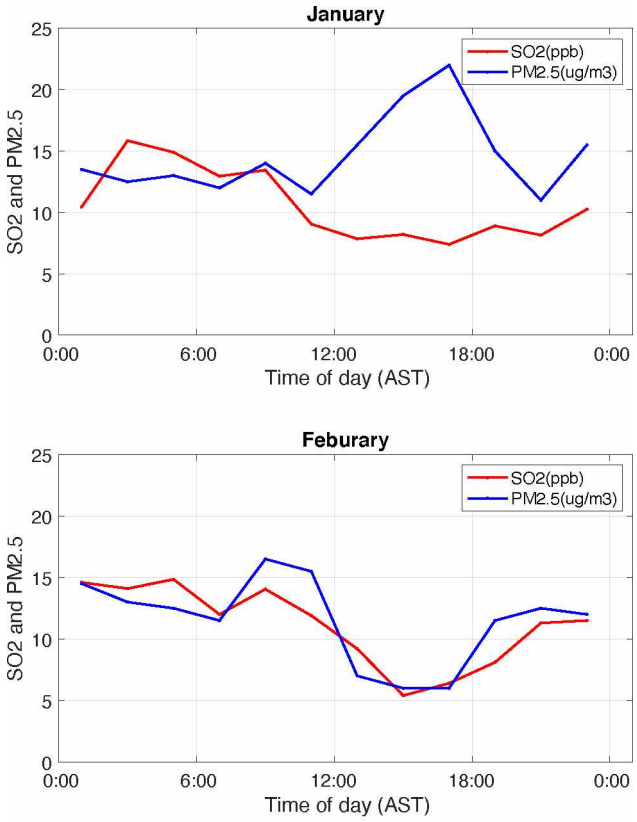

Figure 4.5: Median diurnal variation of hourly SO_2 mixing ration and $PM_{2.5}$ mass concentrations in January (upper) and February (lower) of 2019.

4.4 Median Diurnal Cycles

4.4.1 January Median Diurnal Cycle

To examine the diurnal variation of chemical species, we compute the median values of each hour from the six diurnal cycles collected in January. Figure 4.6 shows that primary pollutants, $PM_{2.5}$, CO, and NO_y show an increasing trend in their diurnal cycles from 10am to 4pm local time. This is likely due to stable boundary layer throughout the day, as a result of lacking sunlight and high solar zenith angle. In particular, lack of surface heating leads to very little vertical mixing and allows primary pollutants to build up throughout the day. Figure 4.6 also shows that $PM_{2.5}$, SO_4^{2-} and NO_3^- all peak in the afternoon, at approximately 4 pm. It is possible that vehicles or heating are potentially causing this afternoon peak. We also see that potassium and carbon monoxide show the same trend of peak times. As both potassium and carbon monoxide are tracers for woodsmoke [*Wang and Hopke*, 2014], this afternoon peak is likely caused by residential heating, and most likely wood smoke. It is also important to point out that the wood smoke factor profile, derived from PMF factor analysis [*Wang and Hopke, 2014*], has very little sulfur contained in this factor.

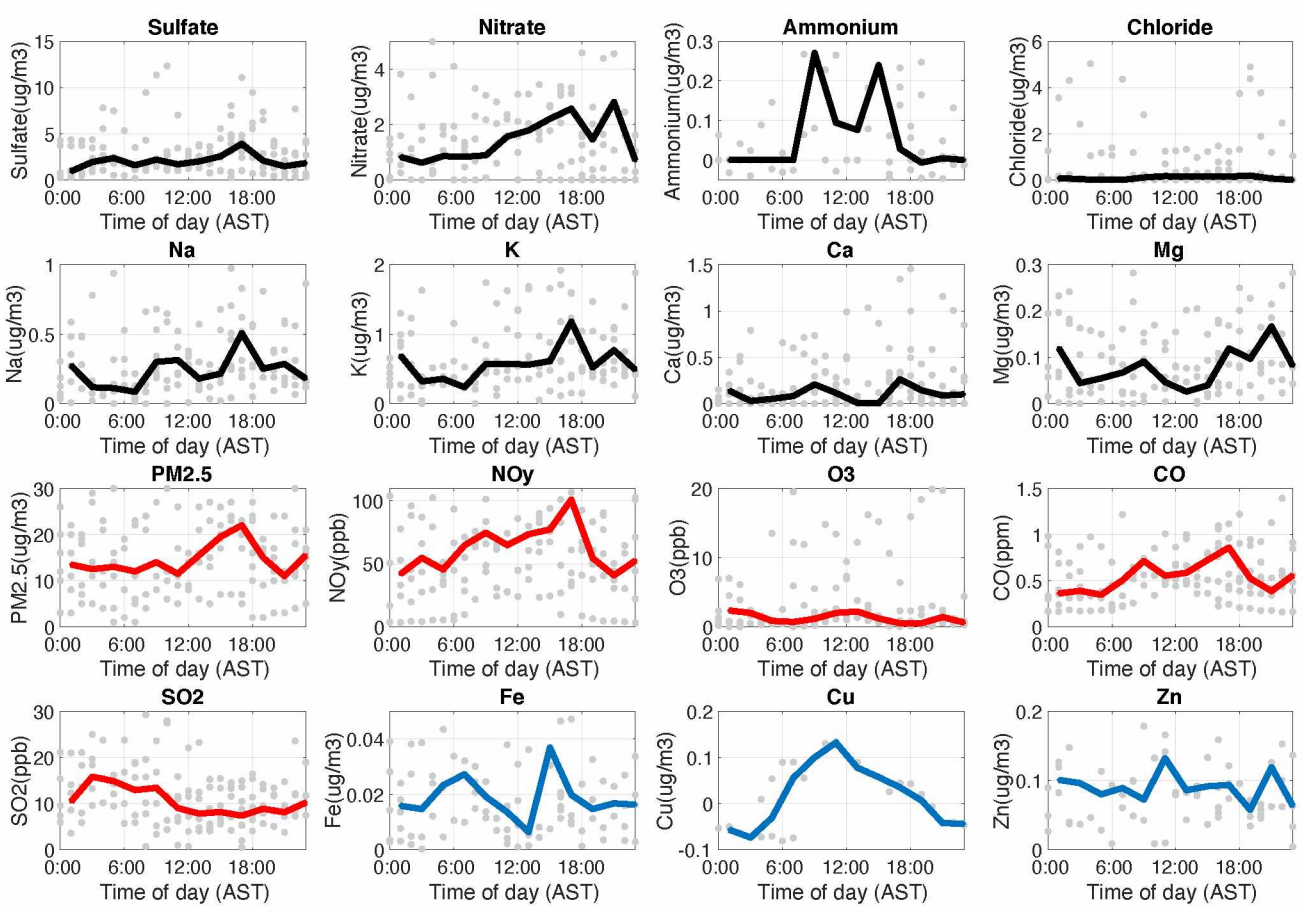

Figure 4.6: Median diurnal cycles of PILS and DEC measurements during January 2019. Individual measurements are presented with gray dots. The black lines indicate data analyzed with the IC and the blue lines indicate data analyzed with the ICP-MS. The red lines indicate data collected by the DEC at the NCore site. Some data points are off the scale so not shown on this figure.

4.4.2 February Median Diurnal Cycle

Similar to January, we compute the median values of each hour from the six diurnal cycles collected in February, as shown in Figure 4.7. In contrast to January diurnal cycles, we see a strong decrease in $PM_{2.5}$, NO_y, and SO_4^{2-} is observed in the afternoon (1pm local time) in February. Most metals and gaseous species show this decrease in concentration in the afternoon as well, except ozone shows a strong increase. This ozone increase in the afternoon is likely resulting from enhanced boundary layer mixing. As the boundary layer height increases by a factor of 2 or 5, the surface pollutant concentrations are largely diluted. In the meantime, surface ozone is replenished by the ozone aloft through entrainment. We emphasize that the diurnal variation in February is in stark contrast to that in January, largely due to stronger vertical mixing in February.

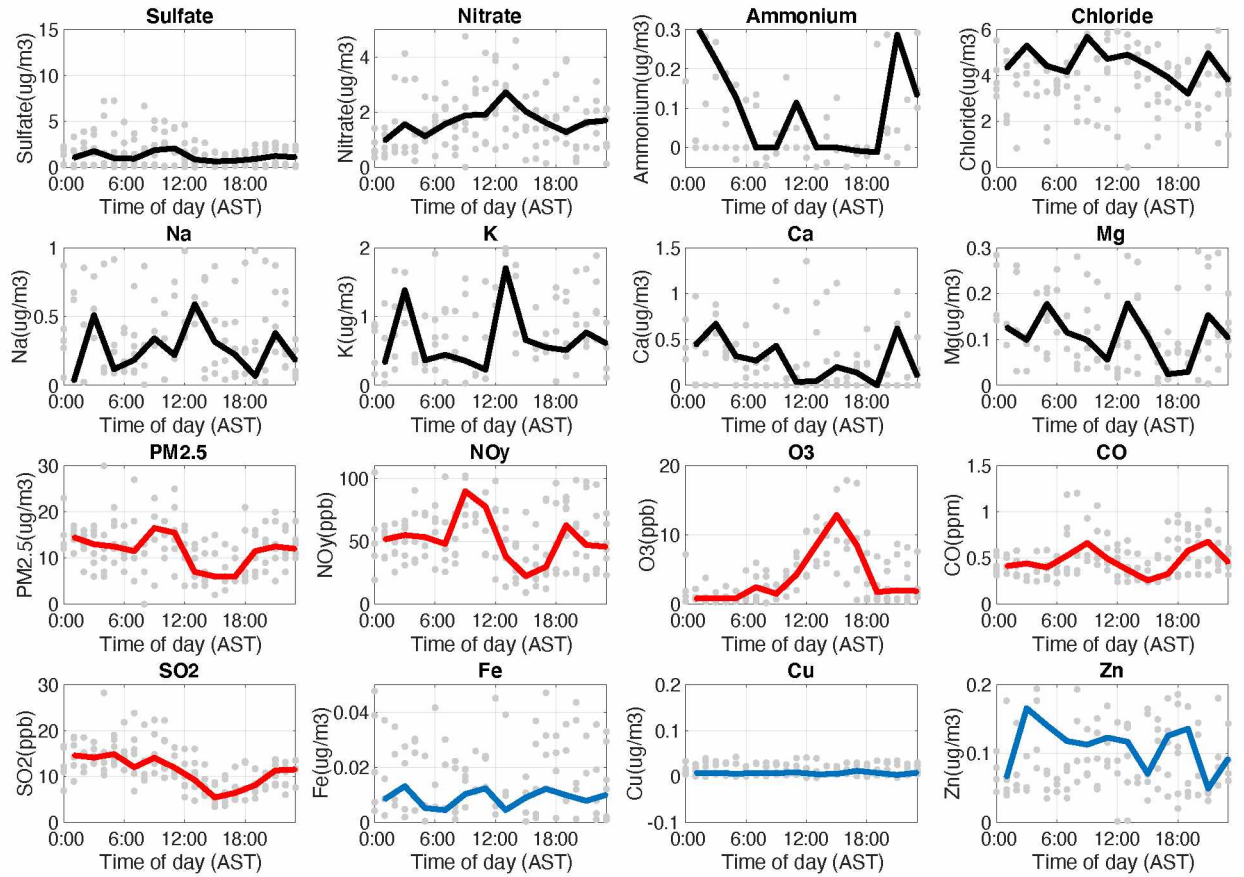

Figure 4.7: Median diurnal cycles of PILS and DEC measurements during February 2019. Individual measurements are presented with gray dots. The black lines indicate data analyzed with the IC and the blue lines indicate data analyzed with the ICP-MS. The red lines indicate data collected by the DEC at the NCore site. Some data points are off the scale so not shown on this figure.

4.5 Inorganic Individual Diurnal Cycle Trends

When analyzing the different diurnal cycles day-by-day as opposed to the total average for each month, we began to see different trends appear. We will discuss these trends in detail in this section.

4.5.1 Loss of Sulfate to $PM_{2.5}$ Correlation

As discussed above, we see a strong correlation between SO_4^{2-} and $PM_{2.5}$ throughout winter. On the coldest diurnal cycle (11-12 Jan) with temperatures reaching -42°C (-44°F), we observe the loss of the strong SO_4^{2-} to $PM_{2.5}$ correlation. We also observe the loss of SO_4^{2-} to $PM_{2.5}$ correlation into February (05-06 Feb, 16-17 Feb and 21-22 Feb). For the February diurnal cycles, Feb 21-22 was the coldest diurnal cycle collected. Figure 4.8 depicts the trend of diurnals showing that we lose the SO_4^{2-} to $PM_{2.5}$ correlation on very cold and warm days.

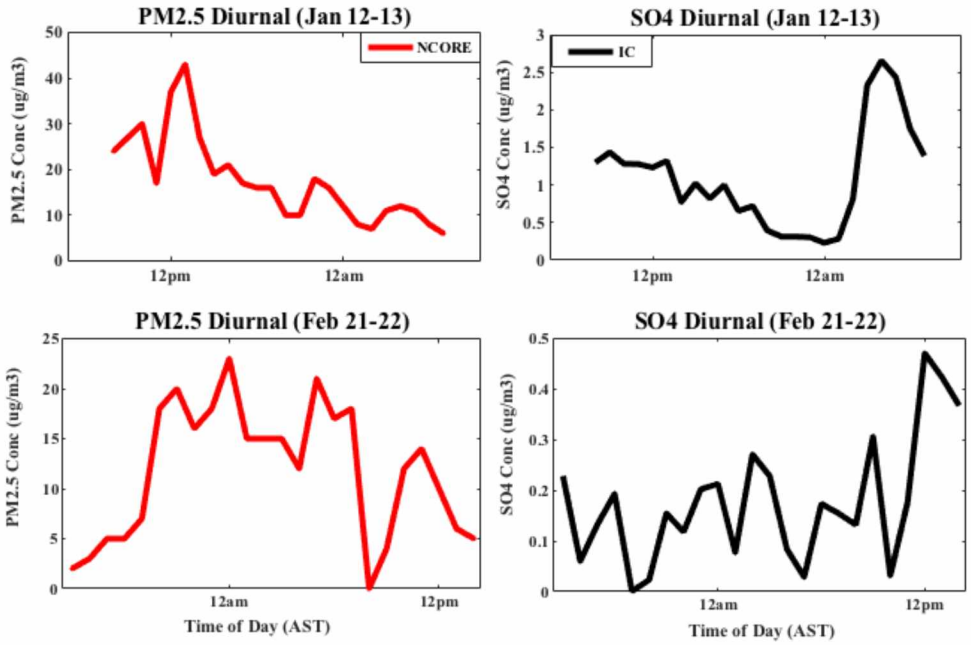

Figure 4.8: Diurnal example of loss of SO_4^{2-} and $PM_{2.5}$ correlation during extreme temperatures. January 12-13 diurnal cycle was the coldest day of Fairbanks winter 2019, with temperatures as low as -42°C. February 21-22 diurnal cycle was the warmest collected samples, with temperatures as warm as 0°C.

Referring to the METAR (Meteorological Terminal Aviation Routine) weather reports and meteorological data collected at the Fairbanks airport (6450 Airport Way) for January 12, 2019, we observe weather conditions of low visibility and mostly cloudy. Ice fog conditions (colder than -34 °C) were observed for the entire morning of January 12th (0:00 – 12:00). While ice fog conditions were not reported at the Fairbanks airport location, it is possible that the mist and cloud covered conditions were observed at the sample site locations, removing particles by precipitation [*Bowling et al.*, 1968].

4.5.2 NH_4 is episodic

In Figure 4.9, we observe that NH_4^+ concentrations and trends can be episodic. At times, SO_4^{2-} and NH_4^+ peak at same time (Jan 15-16). Additionally, $PM_{2.5}$ and NO_y peak at that same time (Jan 15-16). As NH_4^+ peaks with CO or K^+, this NH_4^+ peak is likely due to a combustion source.

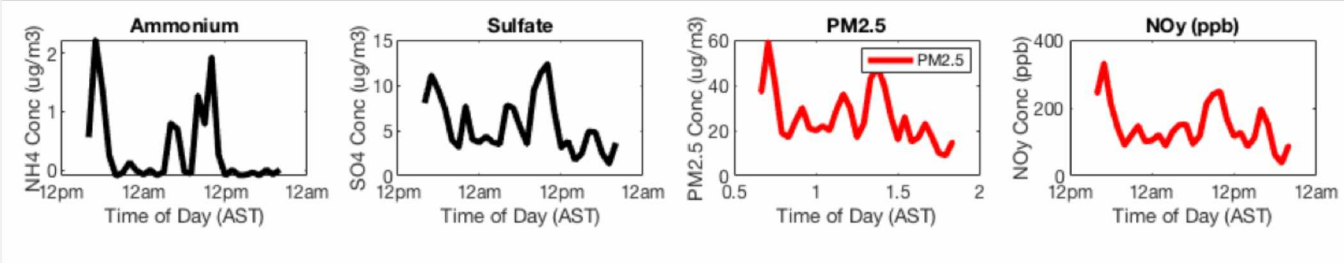

Figure 4.9: NH_4^+ trends and correlation are episodic. In the January 15-16 diurnal cycle, NH_4^+ peaks with SO_4^{2-}, $PM_{2.5}$ and NO_y. This is not observed in most cycles, as seen in the January average diurnal cycle in Figure 4.5.

While research on direct sources of ammonium are limited, biomass burning is a well-documented source of ammonia emissions [*Akagi et al.*, 2011], which suggests that the combustion in woodstoves is a source of NH_3.

4.6 MOUDI Observations

4.6.1 Size distribution of Sulfate and $PM_{2.5}$

Figure 4.10 and Figure 4.11 shows the size distribution of particulate matter throughout Fairbanks winter months, collected by MOUDI. In order to have enough aerosol mass on each filter, we collect filters that are integrated samples over 5-6-day periods. These figures show that most of the particulate matter is submicron.

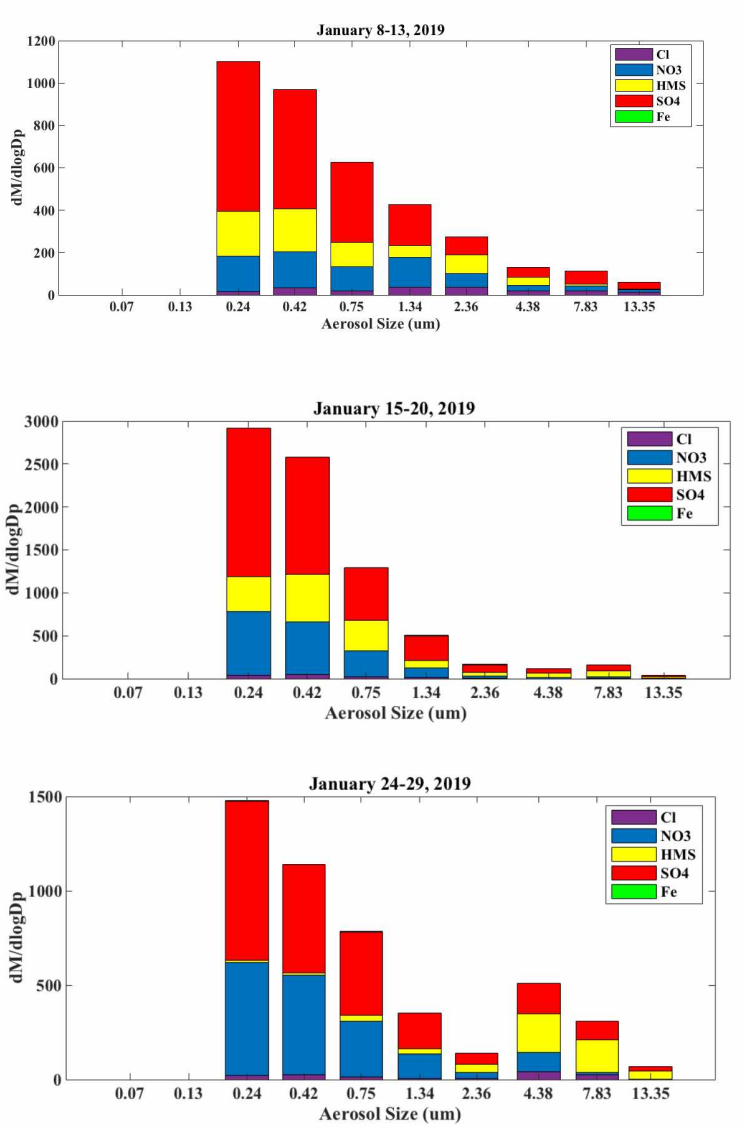

Figure 4.10: January MOUDI size distribution of Fairbanks aerosol particles.

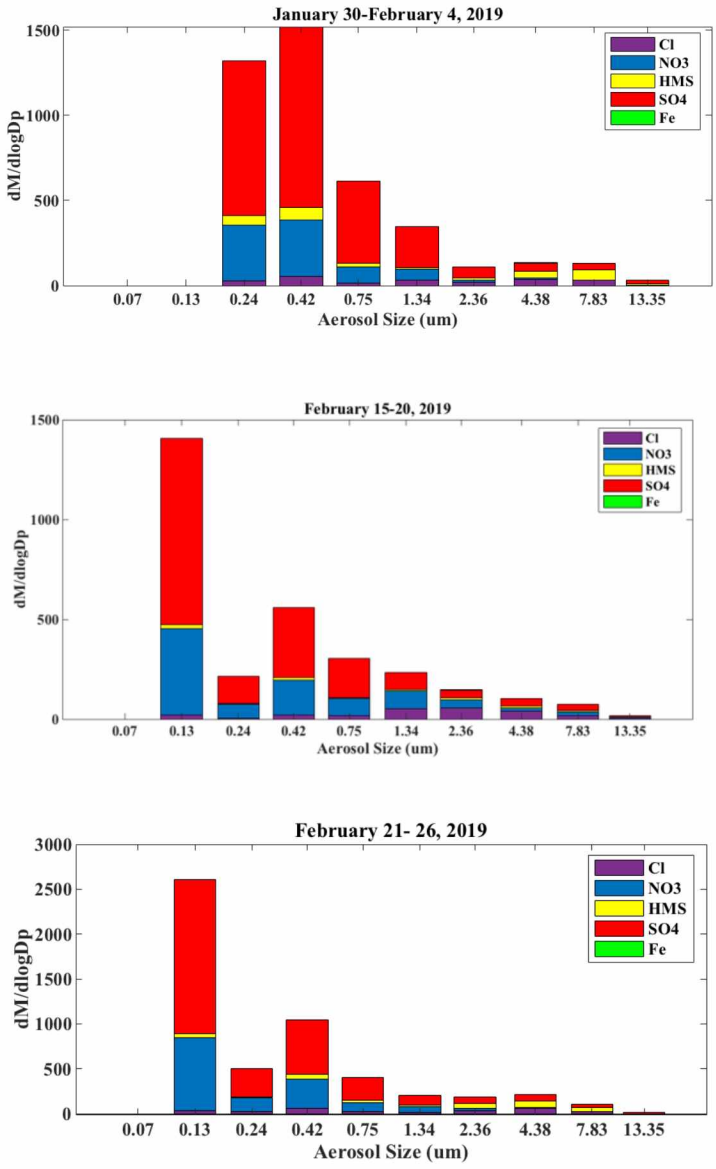

Figure 4.11: February size distributional trends for Fairbanks winter aerosol particles.

4.6.2 HMS in Fairbanks

One major finding from MOUDI samples is the presence of hydroxymethane sulfonate (HMS) in Fairbanks fine particles (Figure 4.11 and 4.12). Several studies have proposed the formation of HMS to explain the difference between modeled and measured submicron sulfate in northern China haze [*Moch et al.*, 2018; *Song et al.*, 2019]. Moch et al. [2018] proposes the following mechanism to take place in cloud droplets following [*Boyce and Hoffmann*, 1984]:

$SO_2(g) \leftrightarrow SO_2\ (aq)$

$SO_2\ (aq) + H_2O \leftrightarrow HSO_3^- + H^+$

$HSO_3^- \leftrightarrow SO_3^{2-} + H^+$

$HCHO(g) \leftrightarrow HCHO\ (aq)$

$HCHO\ (aq) + HSO_3^- \leftrightarrow HOCH_2SO_3^-$

$HCHO\ (aq) + SO_3^{2-} + H_2O \leftrightarrow HOCH_2SO_3^- + OH^-$

Once cloud droplets evaporate, HMS will remain in aerosol and contribute to total sulfur. Song et al. [2019] proposes a mechanism similar to above, but assume the aqueous reactions take place in aerosol phase, and HMS is subsequently converted to sulfate, leading to substantial production of sulfate.

Quantification of HMS in aerosols remains as a challenge. HMS was previously measured by single particle mass spectrometry, as a tracer for fog-processing particles for qualitative analysis [*Neubauer et al.*, 1996; *Whiteaker and Prather*, 2003]. However, the quantification of HMS was recently explored by Ion Chromatography [*Dovrou et al.*, 2019; *Ma et al.*, 2020]. It is found that the detection of HMS is largely dependent on the pH in eluent solution. For a Dionex anion IC with KOH as eluent, the pH in the IC column can higher than 12, largely removing HMS from aqueous phase and potentially converting HMS to sulfate inside IC column, leading to bias in the quantification of HMS.

Our MOUDI samples was analyzed at Rodney Weber group at Georgia Tech. They used a Metrohm IC for their analysis with Na_2CO_3 and $NaHCO_3$ as eluent, with pH close to 8. This low pH largely stabilizes HMS in the IC column and enhances instrument sensitivity to HMS. The calibration of HMS was conducted with commercial sodium hydroxymethanesulfonate (CH_3NaO_4S).

We show in Figure 4.9 and 4.11 that HMS was first time observed in US, contributing to a significant fraction (10-20%) of total sulfur in ambient aerosols during Fairbanks winter. We show from the MOUDI samples collected in the winter of 2019 that HMS is present in the small, fine particulate size bins during very cold temperatures. The coldest sample period collected

during the 2019 winter was -42°C (-44°F) on January 12. Furthermore, it is recognized that during warmer temperatures (late January into February), HMS is observed in the larger size bin categories. Further studies will provide knowledge on what is contributing to HMS formation in different size distributions in addition to how HMS may play a role in the SO_4^{2-} formation reaction.

The presence of HMS is also consistent with a previous study by *Shakya and Peltier* [2013], which shows evidence of missing sulfur species in Fairbanks winter. Shakya et al. [2013] analyzed the total sulfur (S, by XRF) and the sulfate sulfur (SS, by IC) from aerosol filters collected between 2005-2012. They find a discrepancy in the sulfur determined by X-ray fluorescence (S, XRF) spectroscopy to the measured sulfur by ion chromatography (SS, IC) in $PM_{2.5}$. They find this ratio S/SS is great than 1 during Fairbanks winter, suggesting 10-15% of aerosol sulfur is not sulfate. Given the relative fraction of HMS to sulfate, it is likely that HMS may contribute to this missing sulfur compounds in Fairbanks winter.

The presence of HMS in wintertime Fairbanks particles has important implications for aerosol physics and chemistry. It remains unclear whether HMS is formed in cloud droplets, aqueous aerosols, or both. The exact mechanism and drivers (temperature, RH, HCHO, SO_2 etc.) for the formation of HMS remains to be elucidated. It is also unclear whether this HMS is merely a reservoir for SO_2 or serves as a pathway to facilitate sulfate formation.

Chapter 5 Results and Discussion: Metal Species

In this chapter we discuss the metal concentrations from PILS samples collected in January and February of 2019. It is also important to note that all metal concentrations are dissolved metals, since all PILS samples collected were aqueous.

5.1 Sulfate Correlation to Metals

All figures displaying both IC and ICP-MS data (analyses with sodium, magnesium, potassium and calcium) show differing concentrations. Further investigation into the differences between IC and ICP-MS values is discussed in Section 5.4; however, in summary, the instrumentation used to analyze each cation is depicted throughout this results section.

Figure 5.1 shows the correlations between all the metals analyzed with sulfate. Iron, manganese, sodium, magnesium, potassium and calcium all show negative correlation with sulfate in January. Zinc shows slight positive correlation with sulfate in January. Copper from PILS samples was below detection limits during January.

When analyzing metals and sulfate correlation into February (Figure 5.2), we observe stronger correlations between all metals and sulfate relative to January. Zinc, manganese and copper all show positive correlation with sulfate. As discussed in Chapter 4, a stronger correlation between metals and sulfate could be due to the stronger vertical mixing in February, which becomes the major driver of variability for metals and sulfate.

We notice that our metal concentrations (especially for sodium, potassium and calcium) are higher than the filter-based aerosol speciation measurements at NCORE site. Since we have blank subtracted all interfering cations from our 18.2 MΩ sample flow, high values for the PILS metal data are unlikely due to the water source used in sampling and analysis. We further rule out the possibility of the pump exhaust (pumps sit on the roof of sample trailer for filter sampling) interfering with sample collection, by comparing the data between days that pumps

were running and days that pumps were not running. It remains unclear why our metal data appears to be higher than DEC data.

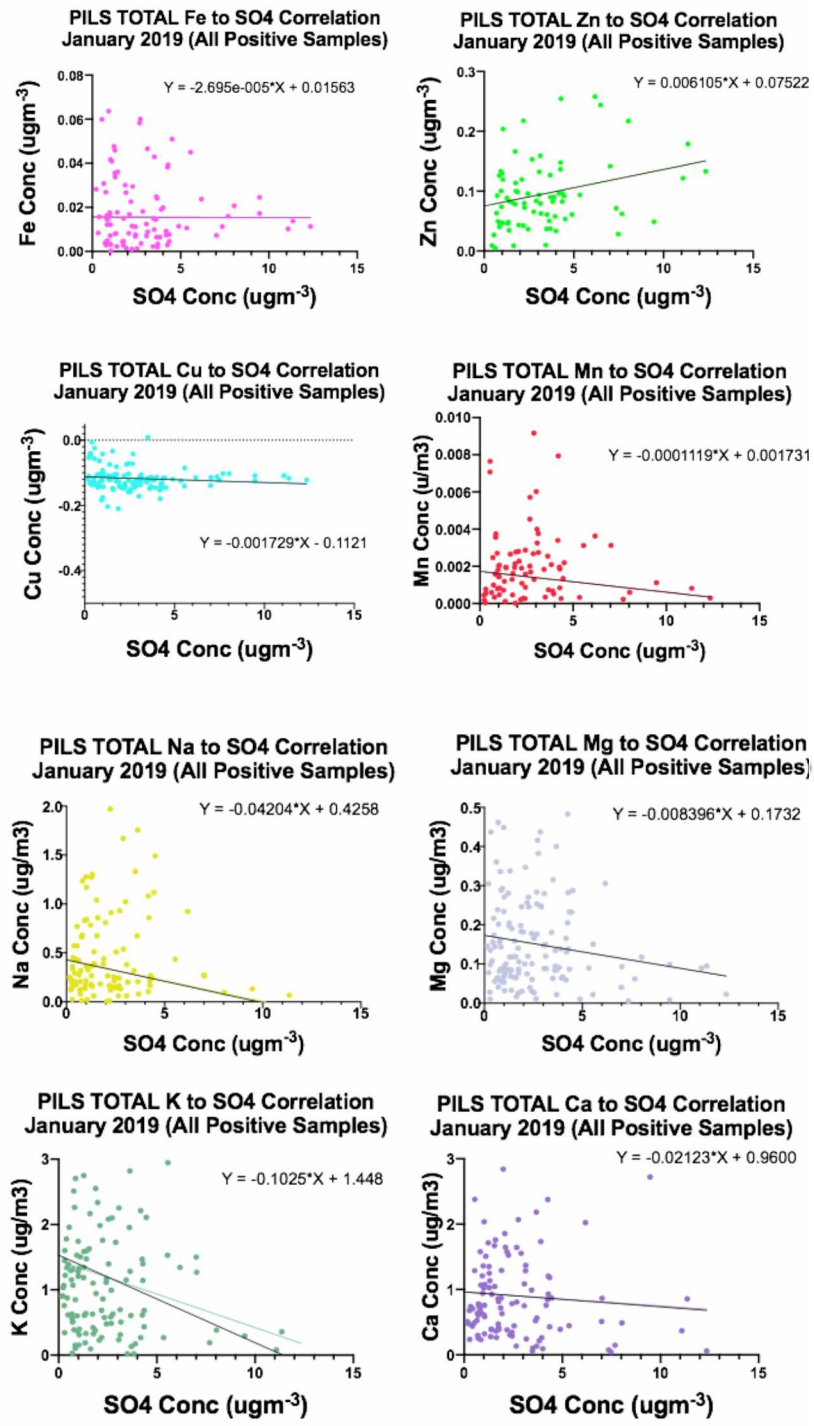

Figure 5.1: Correlation between January SO_4^{2-} to all metals. It is observed that in January, there are not strong linear correlations between sulfate and either metal.

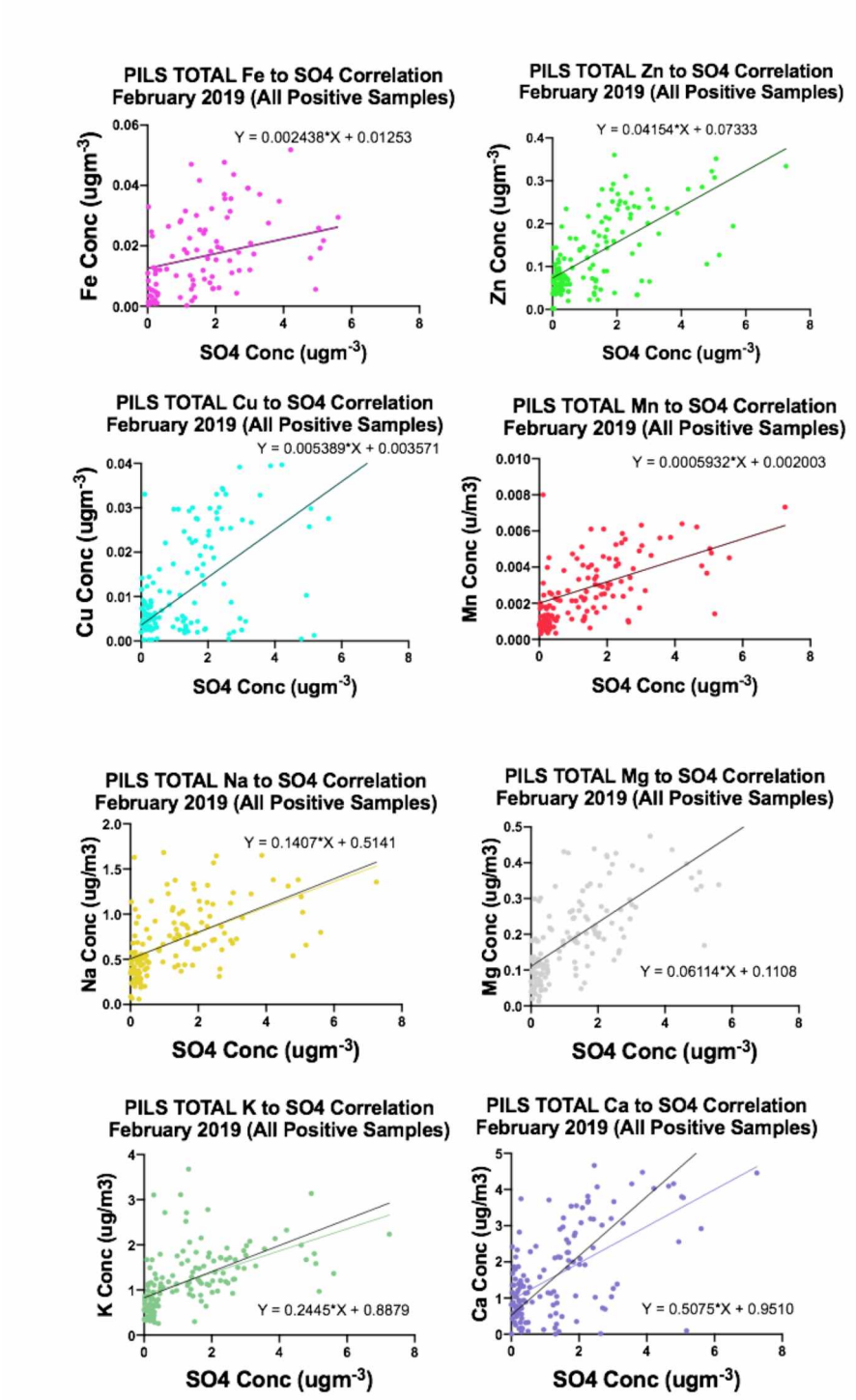

Figure 5.2: Correlation between February SO_4^{2-} and all metals. In February, strong linear correlations are observed for all metals.

5.2 Strontium and Barium to Total $PM_{2.5}$

Figure 5.3 shows both the correlation between strontium/ barium and total $PM_{2.5}$ mass for EPA daily averaged aerosol speciation dataset between 2013-2019, as well as hourly dataset collected by PILS in this study. We only show strontium in January from hourly PILS dataset, as strontium in February is below detection limit. And most barium data from our PILS samples are below detection limit.

We show that there is little correlation between barium and $PM_{2.5}$, or strontium and $PM_{2.5}$. As strontium and barium are considered to be tracers for powerplant emissions, the poor correlation between strontium/ barium and total $PM_{2.5}$ mass shows little influence of coal powerplant emissions to our sampling site.

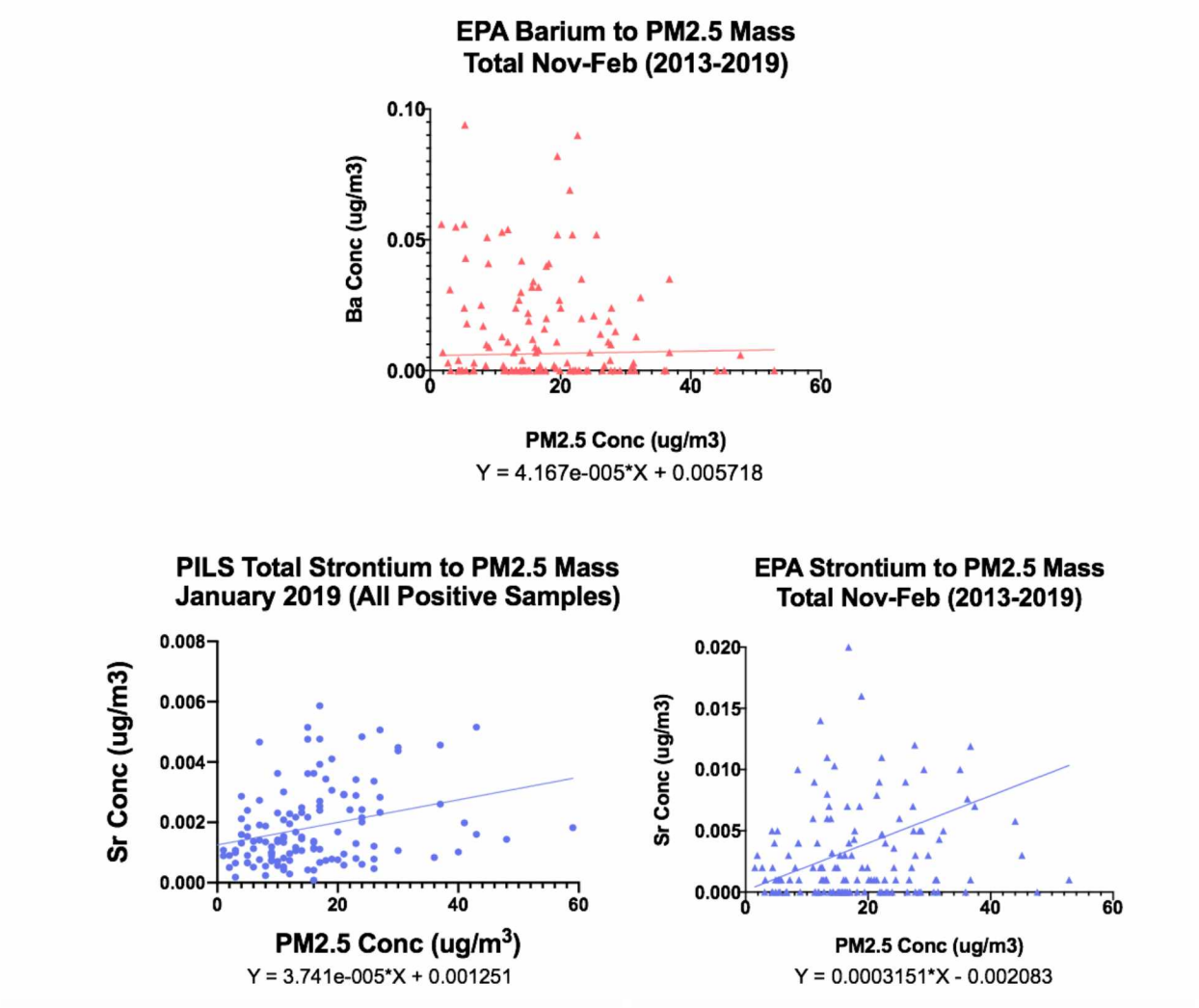

Figure 5.3: Strontium and Barium correlation to $PM_{2.5}$ mass. The scattered correlation between the metals and $PM_{2.5}$ show that there is little evidence for power plant emissions in the boundary layer. Both EPA and diurnal data for strontium is observed. All PILS diurnal samples (January and February) were below detection limits for barium and all February samples were below detection limits for strontium.

5.3 Zn Correlation with $PM_{2.5}$

We observe a strong zinc and $PM_{2.5}$ correlation for both January and February when analyzing EPA data (2013-2019) as well, as shown in Figure 5.4. Zinc is not considered a transition metal, due to the fact that it contains a full filled d-orbital and hence there is not much analysis on if zinc could contribute to SO_4^{2-} secondary formation. When analyzing sources of zinc, we know it

is an additive of motor oil. It is also been hypothesized that automotive repair shops might sell used car oil to businesses in downtown Fairbanks as a cheaper heating source than heating oil.

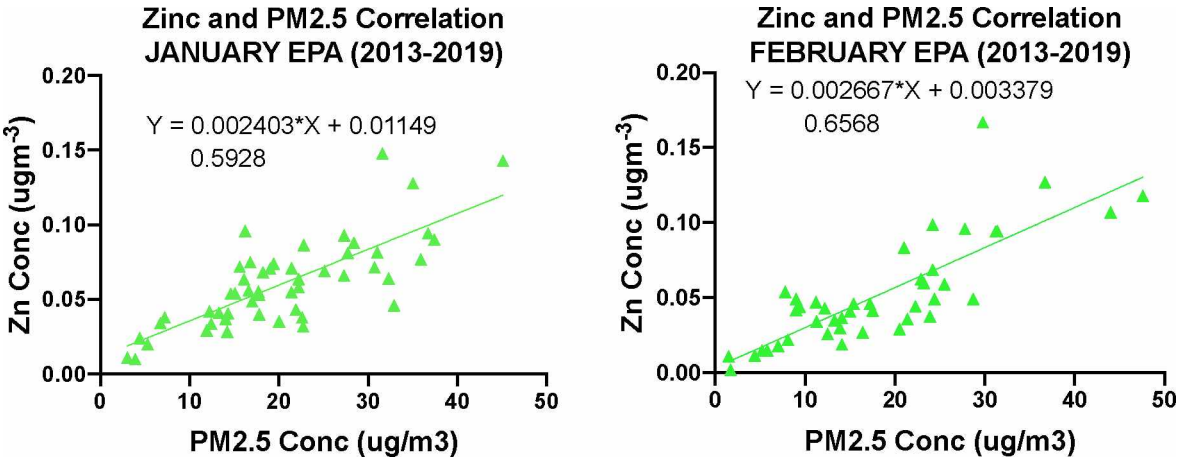

Figure 5.4: $PM_{2.5}$ and Zn EPA 24-hour average scattered correlation.

5.4 ICP-MS versus IC discrepancies

We conducted analysis on metals and cations using both ICP-MS and IC in order to analyze for all desired metals. This analysis lead to some discrepancies in the two instruments, leading to the analysis of the same species by ICP-MS and IC to often differ significantly. Figure 5.5 displays different scatter correlations and R^2 values for potassium and sodium, two cations that are both analyzed using IC and ICP-MS. It is observed that when both species are analyzed using the same instrumentation (IC – IC or ICP-MS – ICP-MS), the correlation values are improved. Because of this, when applicable, each instrument is correlated with that cation values of the same instrument. Because IC was used to analyze anions, when comparing anions to cations, the IC instrument concentration values were used.

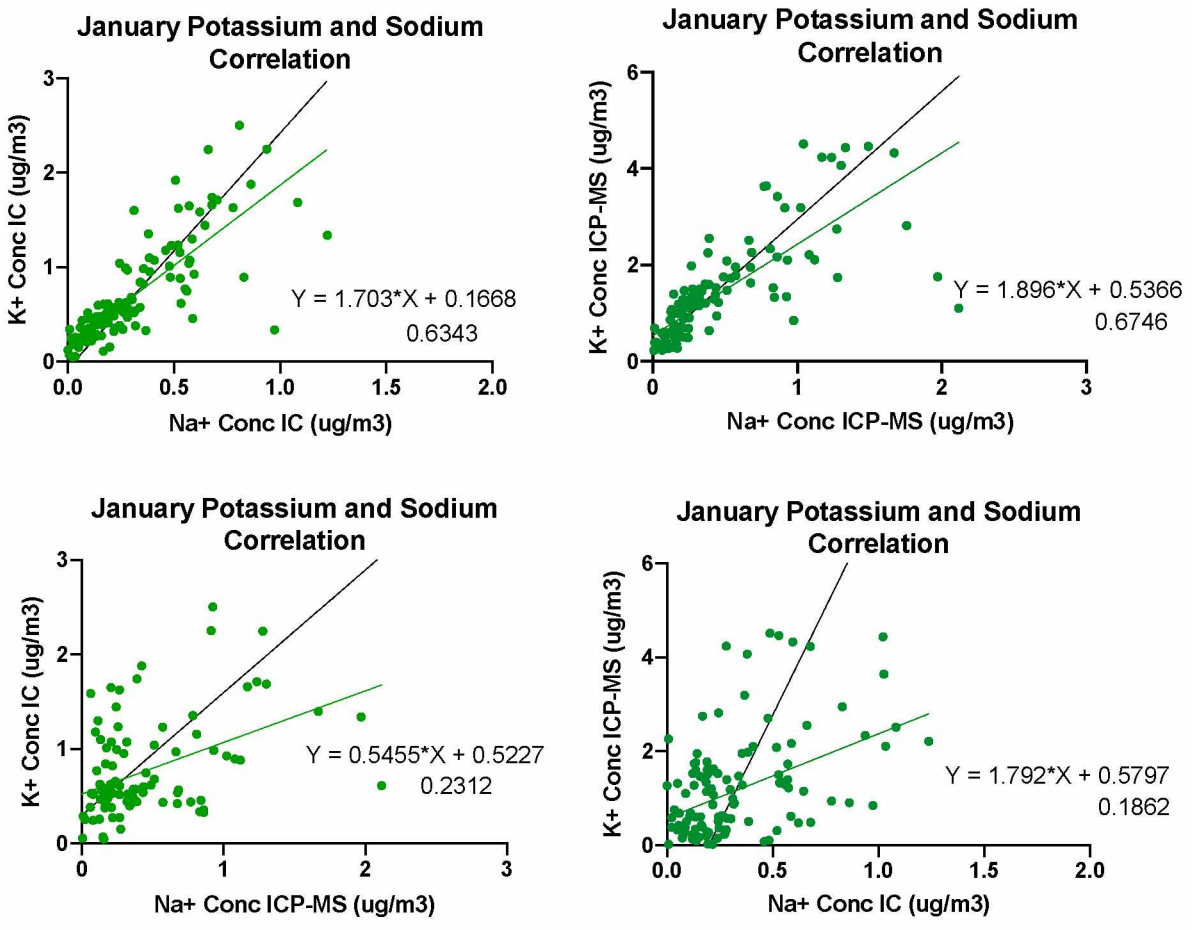

Figure 5.5: Correlation values to determine differences in IC and ICP-MS instrumentation. Potassium and sodium correlation is analyzed using different instrumentation values to determine which instrument is more accurate.

Chapter 6 Conclusions and Future Work

6.1 Conclusions with Regard to this Thesis Study

We collected twelve full diurnal cycles over the winter months of 2019, using a particle-to-liquid sampler (PILS) at hourly time resolution. This PILS instrument creates an aqueous extract containing only the water-soluble components of the aerosol particles. These aqueous extracts were analyzed offline for inorganic and metal concentrations by ion chromatography (IC) and inductively coupled plasma mass spectrometry (ICP-MS). This hourly dataset provides new insights in emissions, chemical processing and their coupling with boundary layer dynamics.

We first show from this hourly dataset that there appears to be a cluster of data with high $PM_{2.5}$ and low sulfate. This cluster data was not found from 24-hr average aerosol speciation data provided by EPA at the same location. As these data points are often accompanied by high level of SO_2, our hourly dataset suggests that this cluster of data are likely due to nighttime plumes of heating oil combustion. It may also suggest that sulfate emission from heating oil is low.

We also find a strong difference between diurnal cycle in January and in February. Due to the strong inversion in January, the diurnal variability of primary pollutants is often driven by source strength. As a result, we see different diurnal patterns between SO_2 and $PM_{2.5}$ in January, likely due to different driving sources. In contrast, we see different diurnal pattern for these primary pollutants in February, with a sharp decrease in the afternoon. This is mainly driven by strong boundary layer mixing in the afternoon, which largely determines diurnal variability for most primary pollutants. These difference in diurnal pattern may have important implications on understanding diurnal variability of chemical species in different months of the winter.

We do not find strong correlation between sulfate and dissolved iron or copper concentrations from PILS hourly samples. On the other hand, we find positive correlation between manganese and sulfate in several diurnal cycles. To what extent TMI catalyze sulfate formation in Fairbanks winter requires further investigation.

A major finding of this study is the presence of HMS in Fairbanks winter. To our knowledge this is the first time HMS measured in Fairbanks area. The presence of HMS is also consistent with previous speculation of missing sulfur compounds in Fairbanks winter. Whether HMS can serve as a sulfur reservoir or facilitate sulfate formation warrants further investigation.

6.2 Future Work

While the diurnal cycles provide further knowledge into the hourly processes occurring throughout the winter, further data on sulfur-containing compounds, such as dibenzothiophene benzonaphthol thiophene, which are known tracers for diesel vehicles and residential oil burners, would help guide the source apportionment of the sulfur sources [*Ward et al.*, 2012]. Diurnal cycles of these sulfur-containing compounds would provide more evidence on what diurnal peaks are source driven and which are potentially secondarily formed.

As discussed previously, the nitrate and metal values for the 12 diurnal cycles collected vary throughout the two months and do not correspond to what is measured by the EPA during the 24-hour average filter sample. The field campaign that is currently collecting samples for the winter of 2020 uses an online PILS-IC near the state office building. The initial online nitrate values collected appear to be much lower in comparison to the offline-PILS-IC samples. This could provide evidence that there was a small contamination with collecting vials that caused nitrate and potentially metal numbers to increase. Furthermore, since nitrate is only stable in aqueous form for 28 days and is susceptible to evaporation [*Harrison et al.*, 1990], the comparison of online versus offline analysis and sample collection will assist in understanding any chemical processes that are not accounted for when samples are pulled from the sub-arctic outside temperatures into a heated trailer. Additionally, this future study will allow us to compare numerical values of all anion species collected and eliminate any potential error associated with transferring vials and samples.

Additionally, after observing the second cluster of sulfate aerosol particles (Figure 4.1), further knowledge of organic carbon diurnal cycles would provide more evidence on source driven sulfate. The relationship between sulfate and woodsmoke can be further explained by analyzing

organic carbon and levoglucosan diurnal cycles, a known chemical tracer of woodsmoke [*Simoneit et al.*, 1999], with sulfate. The total organic carbon diurnal cycles were analyzed with a Total Organic Carbon (TOC) analyzer for the samples collected in this study, but the analyses were concluded ineffective in use of this study.

The measure of water-soluble organic acid (WSOAs) diurnal cycles in comparison with organic and inorganic species would provide more information in regard to the pH of the aerosols, the dependency on relative humidity (RH) [*Yang et al.*, 2017] and the species sources [*Claeys et al.*, 2004; *Hallquist et al.*, 2009; *Tang et al.*, 2020]. It was observed that during highly polluted haze days in China, aqueous-phase secondary reactions was the dominate pathway for WSOAs formation reactions [*Claeys et al.*, 2004]. Additionally, the organic carbon to sulfur ratio has been well studied and can further explain sources [*Hallquist et al.*, 2009], indicating that a further analysis on organic carbon during Fairbanks winters would assist in understanding Fairbanks atmospheric chemical processes.

In response to the HMS compound that was discovered in the samples collected for this thesis, a winter field campaign has started for the winter of 2020 to quantify the HMS concentrations in Fairbanks air. Additionally, this campaign is motivated to collect more samples at different meteorological time points throughout longer months to analyze when HMS is present in Fairbanks. With the knowledge that there is little evidence for transition metal catalyzed reactions for sulfate aerosol particle formation, understanding the role that HMS and formaldehyde play on Fairbanks winter air pollution and sulfate aerosol particle formation is crucial. This study will also collect additional MOUDI samples in order to better understand the size distribution of aerosol particles. This thesis shows the large variation in species size variation, but future studies using MOUDI will assist in better understanding the effects of meteorological and temperature differences on the distribution.

Furthermore, the Alaskan Pollution and Chemical Analysis (ALPACA, https://alpaca.community.uaf.edu) field campaign plans are underway for the winter of 2021. Organized under the international PACES initiative, the project initiative is to close the

knowledge gaps with the present understanding of the atmospheric chemical mechanisms that are occurring under the cold, dark conditions in Fairbanks winters.

The data used and developed as part of this work is archived with this thesis.
Please contact thesis author Ragen M. Davey or advisor Jingqiu Mao for assistance accessing this data or for assistance with any other questions regarding this thesis.

Ragen Davey: rmdavey@alaska.edu
Jingqiu Mao: Jmao2@alaska.edu

References

ADEC (2019a), Alaska Department of Environmental Conservation Website, Division of Air Quality. Available from: https://dec.alaska.gov/air/ (Accessed 03 Feb 2020), 2019a.

ADEC (2019b), 2019 Annual Air Quality Monitoring Network Plan, edited by A. Q. D. Alaska Department of Environmental Conservation, Anchorage, AK.

Akagi, S. K., R. J. Yokelson, C. Wiedinmyer, M. J. Alvarado, J. S. Reid, T. Karl, J. D. Crounse, and P. O. Wennberg (2011), Emission factors for open and domestic biomass burning for use in atmospheric models, *Atmospheric Chemistry and Physics*, *11*(9), 4039-4072, doi:10.5194/acp-11-4039-2011.

Anderson, J. O., J. G. Thundiyil, and A. Stolbach (2012), Clearing the Air: A Review of the Effects of Particulate Matter Air Pollution on Human Health, *Journal of Medical Toxicology*, *8*(2), 166-175, doi:10.1007/s13181-011-0203-1.

Bourne, S. M. (2008), A Climate perspective of observed and modeled surface-based temperature inversions in Alaska, M.S. Thesis, 106 pp, University of Alaska Fairbanks.

Bourne, S. M., U. S. Bhatt, J. Zhang, and R. Thoman (2010), Surface-based temperature inversions in Alaska from a climate perspective, *Atmospheric Research*, *95*(2), 353-366, doi:https://doi.org/10.1016/j.atmosres.2009.09.013.

Bowling, S. A., T. Ohtake, and C. S. Benson (1968), Winter Pressure Systems and Ice Fog in Fairbanks, Alaska, *Journal of Applied Meteorology*, *7*(6), 961-968, doi:10.1175/1520-0450(1968)007<0961:Wpsaif>2.0.Co;2.

Boyce, S. D., and M. R. Hoffmann (1984), Kinetics and mechanism of the formation of hydroxymethanesulfonic acid at low pH, *The Journal of Physical Chemistry*, *88*(20), 4740-4746, doi:10.1021/j150664a059.

Brauer, M., et al. (2012), Exposure Assessment for Estimation of the Global Burden of Disease Attributable to Outdoor Air Pollution, *Environmental Science & Technology*, *46*(2), 652-660, doi:10.1021/es2025752.

Chimonas, M.-A. R., and B. D. Gessner (2007), Airborne particulate matter from primarily geologic, non-industrial sources at levels below National Ambient Air Quality Standards is associated with outpatient visits for asthma and quick-relief medication prescriptions among children less than 20 years old enrolled in Medicaid in Anchorage, Alaska, *Environmental Research*, *103*(3), 397-404, doi:https://doi.org/10.1016/j.envres.2006.08.013.

Claeys, M., et al. (2004), Formation of Secondary Organic Aerosols Through Photooxidation of Isoprene, *Science*, *303*(5661), 1173, doi:10.1126/science.1092805.

Deen, J., Adams, A., Fretts, A., Jolly, S., Navas-Acien, A., Devereux, R., Buchwald, D., and Howard, B. (2017), Cardiovascular Disease in American Indian and Alaska Native Youth: Unique Risk Factors and Areas of Scholarly Need, *Journal of the American Heart Association*, *6*(10), e007576, doi:10.1161/JAHA.117.007576.

Deguillaume, L., M. Leriche, K. Desboeufs, G. Mailhot, C. George, and N. Chaumerliac (2005), Transition Metals in Atmospheric Liquid Phases: Sources, Reactivity, and Sensitive Parameters, *Chemical Reviews*, *105*(9), 3388-3431, doi:10.1021/cr040649c.

Dovrou, E., C. Y. Lim, M. R. Canagaratna, J. H. Kroll, D. R. Worsnop, and F. N. Keutsch (2019), Measurement techniques for identifying and quantifying hydroxymethanesulfonate (HMS) in an aqueous matrix and particulate matter using aerosol mass spectrometry and ion chromatography, *Atmospheric Measurements Techniques*, *12*(10), 5303-5315, doi:10.5194/amt-12-5303-2019.

EPA (2018), United States Environmental Protection Agency. National Ambient Air Quality Standards (NAAQS), doi:https://www.epa.gov/naaqs.

EPA (2019), United States Environmental Protection Agency Website, Air Qual. Database Available from: http://www.epa.gov/ (Accessed 21 October 2019), 2019.

Erkens, R., and M. Kelm (2020), Fine particulate matter: An underestimated cardiovascular risk factor?, *European Journal of Preventive Cardiology*, 2047487319899122, doi:10.1177/2047487319899122.

Hallquist, M., et al. (2009), The formation, properties and impact of secondary organic aerosol: current and emerging issues, *Atmospheric Chemistry and Physics*, *9*(14), 5155-5236, doi:10.5194/acp-9-5155-2009.

Harrison, R. M., W. T. Sturges, A. M. N. Kitto, and Y. Li (1990), Kinetics of evaporation of ammonium chloride and ammonium nitrate aerosols, *Atmospheric Environment. Part A. General Topics*, *24*(7), 1883-1888, doi:https://doi.org/10.1016/0960-1686(90)90520-W.

Holstius, D. M., A. Pillarisetti, K. R. Smith, and E. Seto (2014), Field calibrations of a low-cost aerosol sensor at a regulatory monitoring site in California, *Atmospheric Measurements Techniques*, *7*(4), 1121-1131, doi:10.5194/amt-7-1121-2014.

Joyce, P. L., R. von Glasow, and W. R. Simpson (2014), The fate of NOx emissions due to nocturnal oxidation at high latitudes: 1-D simulations and sensitivity experiments, *Atmospheric Chemistry and Physics*, *14*(14), 7601-7616, doi:10.5194/acp-14-7601-2014.

Kampa, M., and E. Castanas (2008), Human health effects of air pollution, *Environmental Pollution*, *151*(2), 362-367, doi:https://doi.org/10.1016/j.envpol.2007.06.012.

Kankanala, P. (2007), Doppler Sodar observations of the winds and structure in the lower atmosphere over Fairbanks, Alaska, M.S. Thesis, 74 pp pp, University of Alaska Fairbanks.

Kleeman, M. J., J. J. Schauer, and G. R. Cass (1999), Size and Composition Distribution of Fine Particulate Matter Emitted from Wood Burning, Meat Charbroiling, and Cigarettes, *Environmental Science & Technology*, *33*(20), 3516-3523, doi:10.1021/es981277q.

Kotchenruther, R. A. (2016), Source apportionment of PM2.5 at multiple Northwest U.S. sites: Assessing regional winter wood smoke impacts from residential wood combustion, *Atmospheric Environment*, *142*, 210-219, doi:https://doi.org/10.1016/j.atmosenv.2016.07.048.

Lim, S. S., et al. (2012), A comparative risk assessment of burden of disease and injury attributable to 67 risk factors and risk factor clusters in 21 regions, 1990–2010: a systematic analysis for the Global Burden of Disease Study 2010, *The Lancet*, *380*(9859), 2224-2260, doi:https://doi.org/10.1016/S0140-6736(12)61766-8.

Ma, T., et al. (2020), Contribution of hydroxymethanesulfonate (HMS) to severe winter haze in the North China Plain, *Atmospheric Chemistry and Physics Discussions.*, *2020*, 1-17, doi:10.5194/acp-2020-113.

McConnell, R., K. Berhane, F. Gilliland, J. Molitor, D. Thomas, F. Lurmann, E. Avol, W. J. Gauderman, and J. M. Peters (2003), Prospective Study of Air Pollution and Bronchitic Symptoms in Children with Asthma, *American Journal of Respiratory and Critical Care Medicine*, *168*(7), 790-797, doi:10.1164/rccm.200304-466OC.

Miller, K. A., D. S. Siscovick, L. Sheppard, K. Shepherd, J. H. Sullivan, G. L. Anderson, and J. D. Kaufman (2007), Long-Term Exposure to Air Pollution and Incidence of Cardiovascular Events in Women, *New England Journal of Medicine*, *356*(5), 447-458, doi:10.1056/NEJMoa054409.

Moch, J. M., et al. (2018), Contribution of Hydroxymethane Sulfonate to Ambient Particulate Matter: A Potential Explanation for High Particulate Sulfur During Severe Winter Haze in Beijing, *Geophysical Research Letters*, *45*(21), 11,969-911,979, doi:10.1029/2018gl079309.

Mölders, N., and G. Kramm (2010), A case study on wintertime inversions in Interior Alaska with WRF, *Atmospheric Research*, *95*(2), 314-332, doi:https://doi.org/10.1016/j.atmosres.2009.06.002.

Motulsky, H. J., and R. E. Brown (2006), Detecting outliers when fitting data with nonlinear regression – a new method based on robust nonlinear regression and the false discovery rate, *BMC Bioinformatics*, *7*(1), 123, doi:10.1186/1471-2105-7-123.

Nattinger, K. C. (2016), Temporal and spatial trends of fine particulate matter composition in Fairbanks, Alaska, M.S. thesis, 144 pp, University of Alaska Fairbanks.

Neubauer, K. R., S. T. Sum, M. V. Johnston, and A. S. Wexler (1996), Sulfur speciation in individual aerosol particles, *Journal of Geophysical Research: Atmospheres*, *101*(D13), 18701-18707, doi:10.1029/96jd01555.

Orsini, D. A., Y. Ma, A. Sullivan, B. Sierau, K. Baumann, and R. J. Weber (2003), Refinements to the particle-into-liquid sampler (PILS) for ground and airborne measurements of water soluble aerosol composition, *Atmospheric Environment*, *37*(9), 1243-1259, doi:https://doi.org/10.1016/S1352-2310(02)01015-4.

Rodriguez, R., F. Murzyn, A. Mehel, and F. Larrarte (2020), Dispersion of ultrafine particles in the wake of car models: A wind tunnel study, *Journal of Wind Engineering and Industrial Aerodynamics*, *198*, 104109, doi:https://doi.org/10.1016/j.jweia.2020.104109.

Seaton, A., D. Godden, W. MacNee, and K. Donaldson (1995), Particulate air pollution and acute health effects, *The Lancet*, *345*(8943), 176-178, doi:https://doi.org/10.1016/S0140-6736(95)90173-6.

Shakya, K. M., and R. E. Peltier (2013), Investigating Missing Sources of Sulfur at Fairbanks, Alaska, *Environmental Science & Technology*, *47*(16), 9332-9338, doi:10.1021/es402020b.

Simoneit, B. R. T., J. J. Schauer, C. G. Nolte, D. R. Oros, V. O. Elias, M. P. Fraser, W. F. Rogge, and G. R. Cass (1999), Levoglucosan, a tracer for cellulose in biomass burning and atmospheric particles, *Atmospheric Environment*, *33*(2), 173-182, doi:https://doi.org/10.1016/S1352-2310(98)00145-9.

Simoneit, B. R. T., J. J. Schauer, C. G. Nolte, D. R. Oros, V. O. Elias, M. P. Fraser, W. F. Rogge, and G. R. Cass (1999), Levoglucosan, a tracer for cellulose in biomass burning and atmospheric particles, *Atmospheric Environment*, *33*(2), 173-182, doi:https://doi.org/10.1016/S1352-2310(98)00145-9.

Slaughter, J. C., T. Lumley, L. Sheppard, J. Q. Koenig, and G. G. Shapiro (2003), Effects of ambient air pollution on symptom severity and medication use in children with asthma, *Annals of Allergy, Asthma & Immunology*, *91*(4), 346-353, doi:10.1016/S1081-1206(10)61681-X.

Song, S., et al. (2019), Possible heterogeneous chemistry of hydroxymethanesulfonate (HMS) in northern China winter haze, *Atmospheric Chemistry and Physics*, *19*(2), 1357-1371, doi:10.5194/acp-19-1357-2019.

Stölzel, M., S. Breitner, J. Cyrys, M. Pitz, G. Wölke, W. Kreyling, J. Heinrich, H. E. Wichmann, and A. Peters (2007), Daily mortality and particulate matter in different size classes in Erfurt, Germany, *Journal of Exposure Science & Environmental Epidemiology*, *17*(5), 458-467, doi:10.1038/sj.jes.7500538.

Sun, Q., X. Hong, and E. Wold Loren (2010), Cardiovascular Effects of Ambient Particulate Air Pollution Exposure, *Circulation*, *121*(25), 2755-2765, doi:10.1161/CIRCULATIONAHA.109.893461.

Tang, S., X. Zhou, J. Zhang, L. Xue, Y. Luo, J. Song, and W. Wang (2020), Characteristics of water-soluble organic acids in PM2.5 during haze and Chinese Spring Festival in winter of Jinan, China: concentrations, formations, and source apportionments, *Environmental Science and Pollution Research*, doi:10.1007/s11356-020-07714-7.

Tran, H. N. Q., and N. Mölders (2011), Investigations on meteorological conditions for elevated PM2.5 in Fairbanks, Alaska, *Atmospheric Research*, *99*(1), 39-49, doi:https://doi.org/10.1016/j.atmosres.2010.08.028.

Wang, Y., and P. K. Hopke (2014), Is Alaska Truly the Great Escape from Air Pollution? - Long Term Source Apportionment of Fine Particulate Matter in Fairbanks, Alaska, *Aerosol and Air Quality Research*, *14*(7), 1875-1882, doi:10.4209/aaqr.2014.03.0047.

Ward, T., B. Trost, J. Conner, J. Flanagan, and R. K. M. Jayanty (2012), Source Apportionment of PM2.5 in a Subarctic Airshed - Fairbanks, Alaska, *Aerosol and Air Quality Research*, *12*(4), 536-543, doi:10.4209/aaqr.2011.11.0208.

Weber, S. A., T. Z. Insaf, E. S. Hall, T. O. Talbot, and A. K. Huff (2016), Assessing the impact of fine particulate matter (PM2.5) on respiratory-cardiovascular chronic diseases in the New York City Metropolitan area using Hierarchical Bayesian Model estimates, *Environmental Research*, *151*, 399-409, doi:https://doi.org/10.1016/j.envres.2016.07.012.

Wendler, G., and P. Nicpon (1975), Low-Level Temperature Inversions in Fairbanks, Central Alaska, *Monthly Weather Review*, *103*(1), 34-44, doi:10.1175/1520-0493(1975)103<0034:Lltiif>2.0.Co;2.

Wendler, G., and M. Shulski (2009), A Century of Climate Change for Fairbanks, Alaska, *Arctic*, *62*(3), 295-300.

Whiteaker, J. R., and K. A. Prather (2003), Hydroxymethanesulfonate as a tracer for fog processing of individual aerosol particles, *Atmospheric Environment*, *37*(8), 1033-1043, doi:https://doi.org/10.1016/S1352-2310(02)01029-4.

Yang, W., J. Zhang, Q. Ma, Y. Zhao, Y. Liu, and H. He (2017), Heterogeneous Reaction of SO(2) on Manganese Oxides: the Effect of Crystal Structure and Relative Humidity, *Scientific Reports*, *7*(1), 4550-4550, doi:10.1038/s41598-017-04551-6.

Appendices

Appendix A: Ion Chromatography Methods

A.1: Anion Gradient Method

All IC-anion analyses were analyzed on the same gradient method (explained in Table A.1), over twelve different IC analysis runs. The preferred extraction method of anion peaks occurred over a 33-minute gradient method, for the AERS (2mm, 0.25mL min^{-1} isocratic flow, 7 mA current) suppressor used. Eluent (KOH) concentration followed a gradient concentration over the sample analysis (33 min) in order to elute the anion peaks for accurate integration. Lower pressure limit (200 psi) and upper limit (3000 psi) were set to maximize pressure allowed through the anion column (AS18 2x250mm).

Table A.1: Anion Gradient Method

Time (min)	KOH Concentration (mM)	Curve
0.00	Equilibration	
0.00	10.00	5
0.00	Run	
0.00	10.00	5
10.00	10.00	5
25.00	45.00	5
30.00	45.00	5
30.10	10.00	5
33.00	Stop Run	

A.2: Cation Isocratic Method

All IC-cation analyses were analyzed on the same isocratic method to allow for accurate peak integration. The preferred cation elution occurred over a 20-minute isocratic method (1.00 mL min^{-1} isocratic flow). Eluent concentration (20 mM MSA) and suppressor current (88 mA) remained constant over the entire cation analysis. Lower pressure limit (200 psi) and upper limit (3000 psi) were set to maximize pressure allowed through the cation column (CS12 4x250mm).

A.3: Instrument Stability

In order to assure instrument stability over the multiple runs and months used, calibration standards and quality assurance standards were used throughout each analysis, for both the IC and ICP-MS. Table A.2 displays calibration standard linear correlations and R^2 correlation values throughout all twelve diurnal cycles to assure instrument accuracy and stability, where X is the integrated conductivity of the sample peak.

Table A.2 Calibration Standard Linear Correlations for IC and ICP-MS Instruments

Diurnal Cycle Date	**Sulfate (IC anion) Linear Correlation**	**Lithium (IC cation) Linear Correlation**	**Manganese (ICP-MS) Linear Correlation**
	R^2 value	**R^2 value**	**R^2 value**
Jan 9-10, 2019	y = 1.2478x + 0.0915[1]	y = 0.4721x + 0.2035	y = 5.725e-003x -5.141e-001[3]
	0.9924	0.9989	0.9997
Jan 11-12, 2019	y = 1.1087x + 0.1721[1]	y = 0.4721x + 0.2035	y = 5.725e-003x -5.141e-001[3]
	0.9966	0.9989	0.9997
Jan 12-13, 2019	y = 1.1086x + 0.1878[1]	y = 0.4711x + 0.1907	y = 5.725e-003x -5.141e-001[3]
	0.9991	0.9935	0.9997
Jan 15-16, 2019	y = 0.00426x - 0.00206	y = 0.4714x + 0.1436	y = 7.850e-002x +1.003e-003[4]
	0.9998	0.9964	0.9999
Jan 28-29, 2019	y = 0.0043x + 0.0011	y = 0.4724x - 0.5683	y = 7.850e-002x +1.003e-003[4]
	0.9999	0.9981	0.9999
Jan 29-30, 2019	y = 0.0038x - 0.0113	y = 0.5541x - 0.4471	y = 7.850e-002x +1.003e-003[4]
	0.9993	0.9975	0.9999
Feb 5-6, 2019	y = 0.0044x - 0.0004	y = 0.4264x - 0.4568	y = 3.598e-002x -1.190e-002[5]
	0.9998	0.9988	0.9999
Feb 14-15, 2019	y = 0.0043x + 0.0258	y = 0.00165x - 0.000495[2]	y = 3.598e-002x -1.190e-002[5]
	0.9999	0.9997	0.9999
Feb 15-16, 2019	y = 0.0043x + 0.026	y = 0.00159x + 0.0000740[2]	y = 3.785e-002x -1.254e-002
	0.9995	0.9930	0.9998
Feb 16-17, 2019	y = 0.004x - 0.0142	y = 0.00175x - 0.00439[2]	y = 3.785e-002x -1.254e-002
	0.9917	0.9989	0.9998
Feb 21-22, 2019	y = 0.0044x - 0.0032	y = 0.00172x - 0.00405[2]	y = 3.785e-002x -1.254e-002
	0.9997	0.9944	0.9998
Feb 24-25, 2019	y = 0.0043x - 0.0087	y = 0.00170x - 0.00281[2]	y = 3.785e-002x -1.254e-002
	0.9995	0.9986	0.9998

[1] First three anion diurnal cycles were run on a different calibration set; the remaining nine diurnals were analyzed using the same calibration standards.
[2] Last five cation diurnal cycles were run on a different calibration set; the first seven diurnal cycles were analyzed using the same calibration standards.
[3]First three diurnal cycles were run on one ICP-MS calibration set; ICP-MS analyses were analyzed with new calibration standards each sample run.
[4] Second three diurnal cycles were run on a second ICP-MS calibration set.
[5] First two February diurnal cycles were run on a third ICP-MS calibration set; the last four diurnal cycles were analyzed with a final set of calibration standards.

Appendix B: Pearson R Correlation Values

In order for this thesis to provide resources for future correlation analyses, the Pearson R correlation values for each species analyzed in the hourly diurnal cycle samples are shown below in Figures B.1 and B.2. These correlations represent the hourly data averaged over each diurnal cycle for both January and February 2019.

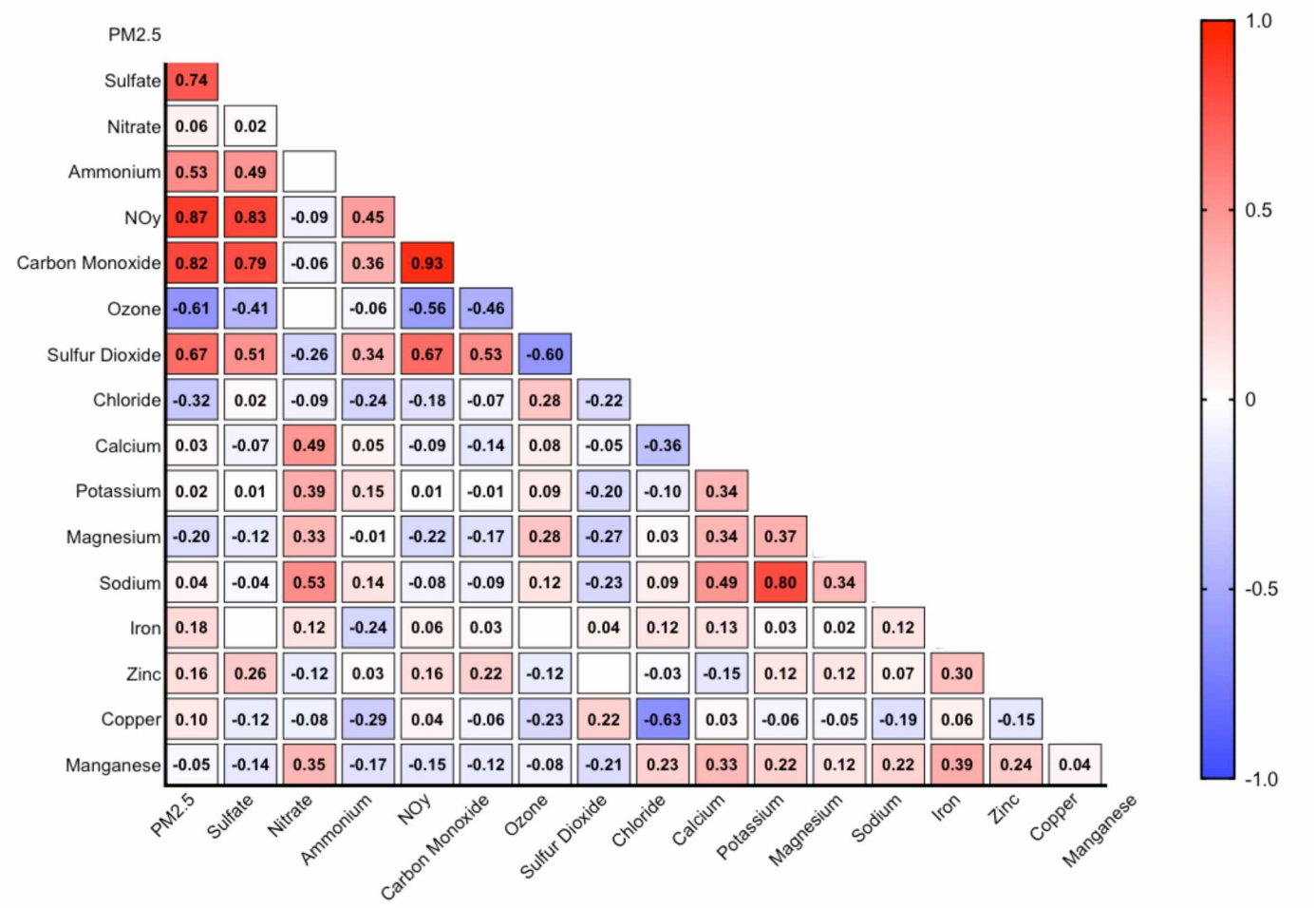

Figure B.1: January Pearson R correlation values for all **averaged** hourly species.

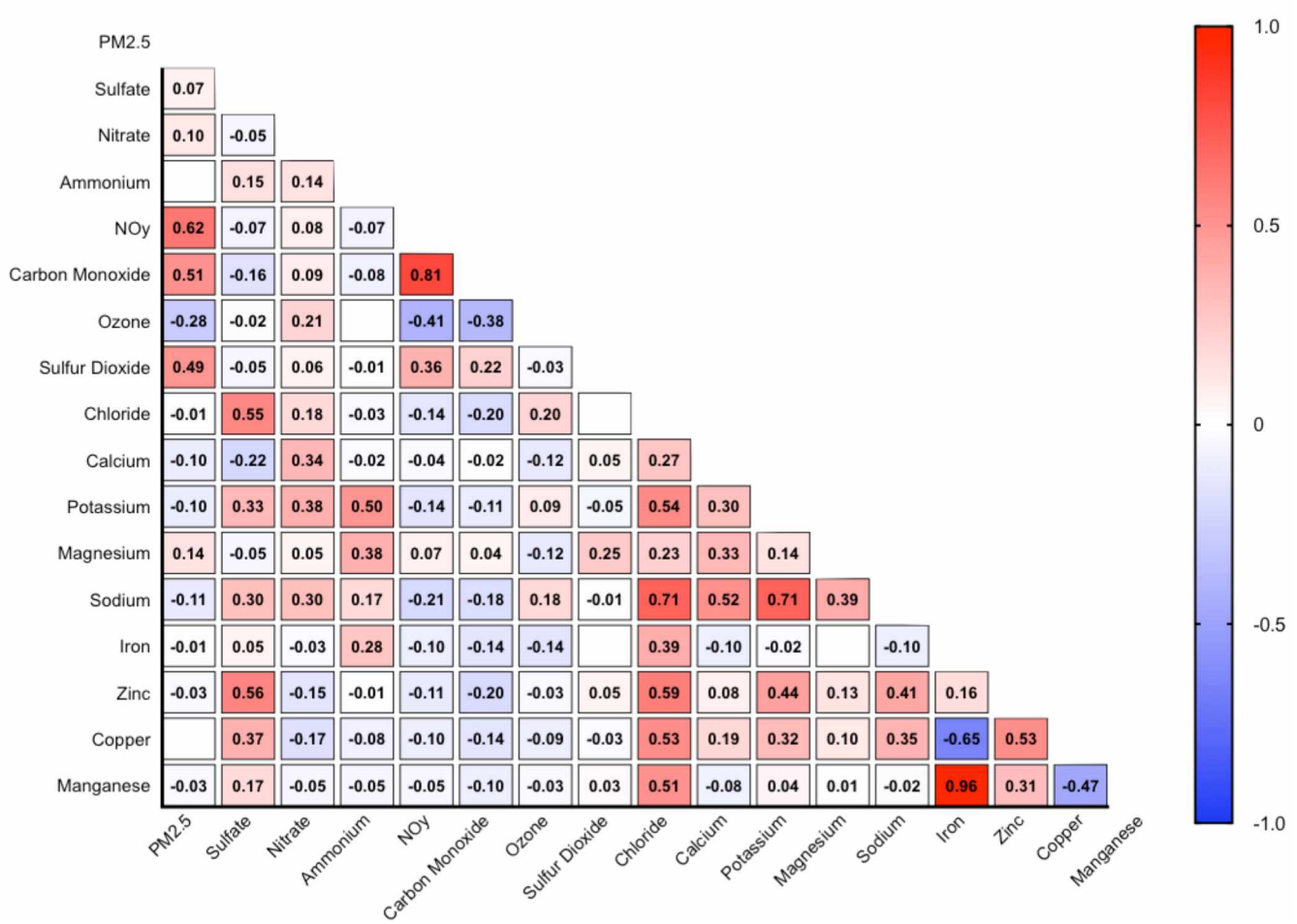

Figure B.2: February Pearson R correlation values for all **averaged** hourly species.

Appendix C: Numerical Data

In order to provide numerical values for each diurnal cycle, the average of PM2.5 and inorganic species and temperature of each diurnal cycle are displayed in Tables C.1 and C.2. The complete data sets used for analysis in this thesis has been archived. Please contact thesis authors for further information.

Table C.1: Average Species Data for January Diurnal Cycles

Jan Diurnal	SO_4 Avg (ug/m3)	NO_3 Avg (ug/m3)	NH_4 Avg (ug/m3)	$PM_{2.5}$ Total Mass	SO_4:NO_3	SO_4% of $PM_{2.5}$	NO_3% of $PM_{2.5}$	NH_4% of $PM_{2.5}$	Avg Temp (°C)
Jan 9-10	1.56	2.34	0.45	6.96	0.67	22%	34%	7%	-25.4
Jan 11-12	2.99	3.48	0.56	17.99	0.86	17%	19%	3%	-34.5
Jan 12-13	1.08	4.08	0.15	16.88	0.26	6%	24%	1%	-29.5
Jan 15-16	5.61	1.64	0.93	25.04	3.42	22%	7%	4%	-21.1
Jan 28-29	1.75	2.23	0.21	12.19	0.79	14%	18%	2%	-4.5
Jan 29-30	2.70	2.17	0.03	11.74	1.24	23%	19%	0%	-9.6
AVG	—	—	—	—	—	17%	20%	2.8%	-20.8

Table B.2: Average Species Data for February Diurnal Cycles

Feb Diurnal	SO_4 Avg (ug/m3)	NO_3 Avg (ug/m3)	NH_4 Avg (ug/m3)	$PM_{2.5}$ Total Mass	SO_4:NO_3	SO_4% of $PM_{2.5}$	NO_3% of $PM_{2.5}$	NH_4% of $PM_{2.5}$	Avg Temp (°C)
Feb 5-6	1.97	3.26	0.85	11.13	0.61	18%	29%	8%	-9.2
Feb 14-15	3.20	1.52	0.45	12.16	2.12	26%	12%	4%	-20.7
Feb 15-16	1.76	1.14	0.31	9.47	1.53	19%	12%	3%	-20.5
Feb 16-17	0.68	1.45	0.12	9.36	0.47	7%	16%	1%	-13.2
Feb 21-22	0.18	2.07	0.45	10.81	0.09	2%	19%	4%	-19.6
Feb 24-25	0.26	2.68	0.72	14.71	0.10	2%	18%	5%	-11.1
AVG	—	—	—	—	—	12.3%	17.8%	4.2%	-15.7